Norwegian University
of Life Sciences

Master's Thesis 2023 30 ECTS
Faculty of Science and Technology

Investigating Competing Phases in GeTe through Phonon Dispersion using Temperature Dependent Effective Potential (TDEP)

Rakel Tzeng-Ohn Steensen
M.Sc. Environmental Physics and Renewable Energy

Preface

This master's thesis marks the end of my five years at the Norwegian University of Life Sciences (NMBU) in Environmental Physics and Renewable Energy. Throughout the years I have attained a lot of knowledge, both inside and outside the classroom. There are therefore some people I would like to thank at the end of this remarkable journey.

I want to thank my two supervisors Kristian Berland and Ole Martin Løvvik for their good support, valuable insights, and constant availability during the course of my master's thesis. Their knowledge in the field, dedication and answers to my never-ending tirade of questions have been uttermost helpful and are very much appreciated. The amazing people proofreading my thesis also deserve attention. You know who you are, and I am forever grateful.

What makes a student other than the relationships and connections created during their period of study? In my mind, not much. Therefore I would like to thank all the people that have made my time at NMBU exciting and fulfilling. This includes my beloved fellow classmates in "Grus". Spending countless hours surrounded by books, papers and computers with all of you was time well-spent. I would also like to thank Åsblæst'n for including me these past 5 years, bringing the social and creative aspects of being a student to life.

Lastly, I would like to thank my friends and family for always being there and supporting me throughout my studies.

Rakel Tzeng-Ohn Steensen
Ås, Mai 2023

Abstract

Germanium telluride (GeTe) has for many years attracted attention because of its good thermoelectric properties. The remarkably low lattice thermal conductivity, despite the simple crystal structure, is an interesting property and gives rise to the question of why. Many thermoelectric materials that are being researched often have more complex crystal structures compared to the diatomic GeTe.

In GeTe a phase transition occurs around temperatures $T = 630$ K ~ 740 K. Previous studies have found that when the trigonal structure is nearing the phase transition, the shape of the structure shifts towards a more cubic structure. This change from a quasi-cubic to a cubic structure is thought to be related to the low lattice thermal conductivity of GeTe.

The effect caused by changing the angle of the trigonal structure of GeTe is what this study investigates, in addition to finding the phase transition. First-principles calculations of the Free energy and phonon dispersion relation have been made at finite temperatures and various trigonal angles using density functional theory (DFT) and temperature dependent effective potential (TDEP). The volumes of the cubic and trigonal cells have been kept constant at the ground state calculated volumes, meaning that the thermal expansion has not been included.

Precise force constants were found using an iterative process where the new iteration is built on the calculations of the previous iterations. This method was successful at improving the precision of the force constants, as high precision is necessary for phonon calculations.

This study shows that the volume of the unit cell is very important when calculating the Free energy. In addition to this, it is important to optimise the atomic positions in the trigonal unit cell. This is because the atomic positions influence the phonon dispersion much. Therefore, to be able to describe the phase transition and dispersion relation of GeTe precisely, temperature, volume, angle and atomic position need to be taken into consideration. In this thesis, only temperature and angle have been included meaning the results are somewhat insufficient in describing the phonon dispersion relation at the phase transition.

In addition to the complexity of the system, the findings suggest that as the temperature decreases, the cubic structure exhibits phonon softening and broadening. This indicates that there is a phase transition occurring in GeTe and that near the phase transition the lattice thermal conductivity is low.

Sammendrag

Germanium tellurid (GeTe) har i mange år fått mye oppmerksomhet på bakgrunn av dens gode termoelektriske egenskaper. Den lave gitterledningsevnen, tross den enkle krystallstrukturen, er svært interessant og gjør at man stiller seg spørsmålet om hvorfor dette er tilfellet. Forskning på termoelektriske materialer gjøres ofte på mer komplekse krystallstrukturer enn diatomiske GeTe.

GeTe opplever en faseovergang ved temperaturene $T = 630$ K ~ 740 K. Tidligere studier har funnet at når det trigonale fasen nærmer seg faseovergnagstemperaturen, endrer den trigonale enhetscellen seg til å bli mer kubisk formet. Denne endringen fra en kvasi-kubisk til en kubisk struktur, er ment å være tilknyttet årsaken til den lave gitterledningsevnen i GeTe.

Effekten fra å endre vinkelen til den trigonale strukturen i GeTe er hva som undersøkes i denne studien, samt å finne faseovergangen. Førsteprinsipps beregninger av Fri energi og fonondispersjonsrelasjonen ved endelige temperaturer og forskjellige vinkler er gjort med tetthetsfunksjonalteori (DFT) og temperaturavhengige effektive potensialer (TDEP). Volum til de kubiske og trigonale cellene er holdt konstant ved grunntilstandsvolumen, noe som betyr at termisk ekspansjon ikke er medberegnet.

Presise kraftkonstanter er funnet ved bruk av en iterativ prosess, der den nye iterasjonen er bygd på beregningene fra de forekommende iterasjonene. Metoden var vellykket med å øke presisjonen til kraftkonstantene, noe viste seg å være nødvendig ved fononberegniner.

Studien viser at volum til enhetscellen er svært viktig for fri energi-beregninger. I tillegg til dette er det viktig å optimalisere atomposisjonene i den trigonale strukturen. Dette ble ikke gjort automatisk under relaksering. Årsaken å inkludere atomposisjonene er at de har stor innvirkning på fonondispersjonen. Dette fører til at temperatur, volum, vinkel og atomposisjoner må tilpasses for beregning av GeTe faseovergangen og fonondispersjonen. I dette studiet har kun temperaturen og vinkelen blitt inkludert, noe som har medført at resultatene fra dispersjonsrelasjonen er noe mangelfull i sin beskrivelse av faseovergangen.

I tillegg til å vise kompleksiteten til GeTe, viser funnene i studien at når temperaturen synker, opplever den kubiske strukturen fononmykning og fononspredning. Dette indikerer at det det skjer en faseovergang i GeTe, og at ved faseoverganger er gitterledningsevnen lav.

Contents

Preface i

Abstract ii

Sammendrag iii

List of Tables vi

List of Figures ix

Acronyms x

1 Introduction **1**

2 Theory **4**

2.1 Germanium Telluride 4

2.2 Lattice dynamics 4

2.2.1 Crystal structure 5

2.2.2 The direct and reciprocal lattice 7

2.2.3 Phonons 8

2.3 Phase transition 13

2.3.1 Free energy 13

2.3.2 First-and second-order phase transition 14

3 Computational methods **16**

3.1 Density functional theory 16

3.1.1 Kohn-Sham density functional theory 16

3.2 Temperature dependent effective potential 18

3.2.1 Model Hamiltonian 19

3.2.2 Free energy 20

3.2.3 Canonical configurations 20

3.2.4 Iterative process of finding force constants 21

3.2.5 TDEP implementation 22

3.3 The calculations 23

3.4 Software 24

3.4.1 VASP and Atomic Simulation Environment . . . 24
3.4.2 PYTHON packages . . . 24
3.5 Calculation details . . . 24
3.5.1 Convergence tests . . . 24

4 Results **31**
4.1 Choice of functional and energy surface . . . 31
4.2 Phase transition . . . 34
4.2.1 Temperature change . . . 35
4.2.2 Angle change . . . 37
4.2.3 Comparison at 700 K . . . 38
4.3 Phonon dispersion relation . . . 40
4.4 Phonon dispersion relation with broadening . . . 43

5 Discussion **44**
5.1 Evaluation of the computational methods . . . 44
5.1.1 Functionals . . . 44
5.1.2 Changing the angle . . . 44
5.1.3 Convergence of the force constants . . . 46
5.1.4 Volume considerations . . . 47
5.2 Phase transition . . . 49
5.3 Phonon dispersion relation . . . 50
5.4 Further work . . . 51

6 Conclusion **52**

A PYTHON script **58**
A.1 Changing the trigonal angle . . . 58

B Convergence tests **59**
B.1 Force constants . . . 59

C Trigonal dispersion relation **61**

List of Tables

2.1 The characteristics of the cubic and trigonal unit cells [18]. 6

3.1 The number of neighbouring atoms at different cutoff radii r_c for the cubic structure. 29

4.1 Calculated ground-state (0 K) and experimental structural parameters for the trigonal phase of GeTe. Four different GGA functionals and one vdW-DF functional were used for the calculations. The experimental data have been found at [10, 13, 55] 32

4.2 The shortest distances between the Ge and Te atoms in a selection of unit cells. The distances have been found using ASE. 34

List of Figures

1.1 Illustration of the Seebeck effect. The electric field is represented by the arrow and the electrons are represented by the e^- symbols. 1
1.2 GeTe as the (a) angle (b) lattice thermal conductivity changes as functions of temperature. The black solid lines represent the phase transition. The figures are adapted from [8, 9]. 3

2.1 Three possible ways of representing the face-centered cubic (FCC) structure of germanium telluride (GeTe). The unit cells are (a) a primitive cell, (b) a conventional cell and (c) a supercell. The supercell in (c) contains 4 conventional cells. 5
2.2 The (a) cubic and (b) trigonal conventional unit cell geometries, with α and a being the angle and lattice constant respectively. 6
2.3 The Brillouin zone of the cubic phase of GeTe with symmetry group $Fm\bar{3}m$. The high symmetry points are marked with filled and unfilled circles. The figure is adapted from the Bilbao Crystallographic Server [22, 23]. 8
2.4 A diatomic linear chain. The masses m and M are alternating, with $m < M$. $2a$ is the length of the unit cell. 9
2.5 The dispersion relation for a diatomic linear lattice showing the optical and acoustical branches. The lattice constant is of length $2a$. 10
2.6 Dispersion relation of trigonal GeTe with broadening at $T = 700$ K. 12
2.7 Phonon softening around the Γ-point for cubic GeTe. 13
2.8 Phase transition is visualised by the difference in Helmholtz Free energy between structure A and structure B. Under the red dashed line, structure A is the most stable, and over the red line structure, B is the most stable state. In the intersection between the red and the blue line, a phase transition occurs at the critical temperature T_c. 14
2.9 Illustration of a (a) first-order phase transition and a (b) second-order phase transition as the temperature changes. The figure is adapted from [28]. . . 15

3.1 Visualisation of three different canonical configurations created from the input supercell in (a). The dashed square represents a unit cell. The different coloured circles are different atoms. 21
3.2 The iterative process of finding converged force constants. The first iteration of canonical configurations is built on fake force constants generated from the Debye temperature. The proceeding iterations are created based on the accumulated force constants from previous iterations. Each *conf000n* is a separate DFT calculation on the GeTe supercell. 22

3.3 The process of using TDEP. A converged and relaxed primitive unit cell is used to find the Debye temperature. A supercell is created from repetitions of the primitive cell, before calculating force constants. After finding the force constants, lattice dynamics like the dispersion relation and Free energy can be calculated. The process of converging the force constants can be seen in Figure 3.2. 23
3.4 Convergence tests of the forces for the functionals PBE, PBEsol, SCAN and vdW-DF-cx for the energy cutoff. Figure (a) and (b) is for the trigonal and cubic primitive cell respectively. The blue dashed line represents the convergence criterion for the forces at $F = 5$ meV/Å. 25
3.5 How the Free energy per atom for the trigonal supercell at 600 K changes with the number of atoms in the supercell. 27
3.6 The intensity states of one mode at the high-symmetry point L for a constant third-order cutoff $r_{c,3} = 5$ Å and different second-order radius cutoffs. 28
3.7 The intensity states for one mode at the high-symmetry point L when keeping $r_{c,2}$ constant and changing $r_{c,3}$. 29

4.1 DFT calculations for the three functionals PBE, PBEsol and vdW-DF-cx with varying angles. The dashed line represents the experimentally found value for the angle at 300 K [13]. The angels are conventional cell angles. . 33
4.2 Contour plot showing the energy landscape in 2D (a) and 3D (b) for trigonal GeTe at $T = 0$ K using the vdW-DF-cx functional. The angles and lattice constants are for the conventional unit cell. 33
4.3 The preferred unit cell angle when relaxing the trigonal structure at $T = 0$ K while holding the volume fixed. The values for volume and angle are for the primitive unit cell. 34
4.4 The difference in Free energy between the cubic and the trigonal structure. The orange points and line are the calculated values and the linearly fitted curve for the first iteration force constants. Similarly for the blue coloured line and points, but for the last iteration force constants. The area over the red line indicates a cubic phase, while the area under the line is the trigonal phase. 35
4.5 The convergence of force constants for the (a) trigonal and (b) cubic structure at various temperatures. The convergence criterion $\Delta F = 0.5$ meV/atom is marked with an orange dashed line. 36
4.6 Calculated Free energy with a fitted curve at the temperatures $T = 500$ K, 600 K and 700 K over a range of angles. 38
4.7 Comparison of the different calculated energies at 700 K. The calculations of the trigonal structures are all at constant volumes and are marked with blue points. The red marks are for the cubic structure with a fully relaxed primitive cell and a cell with the same volume as the trigonal cells. The fully relaxed trigonal structure with ground state structural parameters is used as the baseline. 39
4.8 The dispersion relation for the cubic structure for 5 different temperatures with (a) first iteration force constants and (b) last iteration force constant. . 40
4.9 The phonon dispersion relation for the trigonal structure at three different cell shapes and constant volume. The calculations are at a temperature $T = 600$ K. 41
4.10 The dispersion relation of the trigonal structure with angle $\alpha = 90°$ (red), and the relaxed (blue) and enlarged (purple) cubic structures. The calculations were made at $T = 700$ K. 42

4.11 The phonon dispersion relation plot with smearing for the (a) cubic and (b) trigonal phase of GeTe. The calculations were made at $T = 700$ K. 43

5.1 Illustration of how the atoms in the trigonal unit cell have not moved when the shape of the cell is changed. α is the angle. The green circle is Ge, while the orange is Te. 45
5.2 Illustration over the atomic positions in the (a) cubic unit cell and (b) trigonal unit cell with an angle $\alpha = 90°$ 46

B.1 Convergence of the force constants at $T = 500$ K for different angles. The orange dashed line is the threshold at $\Delta F = 0.5$ meV/atom. 59
B.2 Convergence of the force constants at $T = 600$ K for different angles. The orange dashed line is the threshold at $\Delta F = 0.5$ meV/atom. 60
B.3 Convergence of the force constants at $T = 700$ K for different angles. The orange dashed line is the threshold at $\Delta F = 0.5$ meV/atom. 60

C.1 The dispersion relation for the trigonal structure at 5 different temperatures with (a) first iteration force constants and (b) last iteration force constants. 61

Acronyms

ASE Atomic Simulation Environment

BOA Born-Oppenheimer approximation

DFT density functional theory

DOS density of states

FCC face-centered cubic

FWHM full width half maximum

GeTe germanium telluride

GGA generalised gradient approximation

KS-eq Kohn-Sham equation

LDA local density approach

PAW projector augmented wave

PBE Perdew-Burke-Ernzerhof functional

SE Schrödinger equation

TDEP temperature dependent effective potential

VASP Vienna *ab initio* Simulation Package

vdW van der Waals

Chapter 1

Introduction

The world is in constant need of more energy. According to the United Nations, there are 46 least developed countries [1] and the availability of energy is an important factor for them to develop further. With the environmental impact of using fossil fuels, there is a need to look for other ways to accommodate this demand. A solution might be to find new resources or to improve on already existing ones.

Thermoelectricity might be part of the solution in solving the energy shortage problem. Thermoelectric materials were first discovered around 1820. It was found that certain materials can deflect a compass needle when there is a temperature gradient going the material [2]. Later it have been discovered that there are two thermoelectric effects, the Seebeck and the Peltier effect, working in opposite ways of each other.

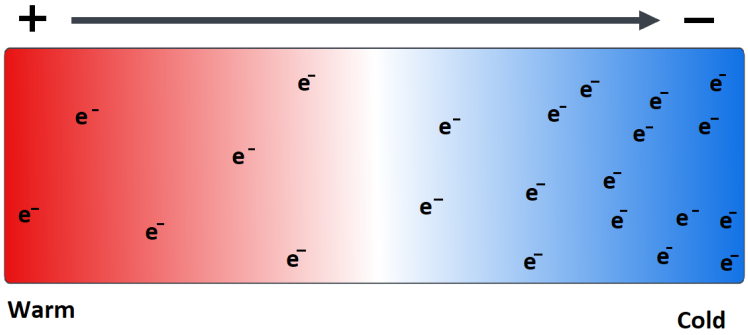

Figure 1.1: Illustration of the Seebeck effect. The electric field is represented by the arrow and the electrons are represented by the e^- symbols.

The Seebeck effect is the generator of the two thermoelectric effects and can be viewed in Figure 1.1. When electrons thermally diffuse from the hot end to the cold end of a thermoelectric material a voltage difference between the two ends will appear. This voltage difference can be used to generate electricity. The Peltier effect is the opposite, meaning that a current, or a voltage difference, will move electrons from the cold side to the warm side creating a temperature difference [2]. This effect can be used in coolers such as refrigerators and in cars [3].

How well a thermoelectric material performs is described by the unitless thermoelectric

figure of merit (ZT)

$$ZT = \frac{\sigma S^2 T}{\kappa_e + \kappa_l}. \tag{1.1}$$

Here the electrical conductivity σ, Seebeck coefficient S and the electron thermal conductivity κ_e all depend on the thermally diffusing electrons in the material. This means that when engineering the material to optimise one of these quantities, all the other quantities also get affected. The last two parts are the temperature T and the lattice thermal conductivity κ_l [4].

The lattice thermal conductivity κ_l is, as the name implies, dependent on the lattice dynamics of the system and not the movement of electrons. The atoms in the crystal lattice vibrate, and their periodic collective vibration is called phonons [5]. It is the phonons that are responsible for the heat transport in the lattice, and the main focus of this thesis.

Suitable thermoelectric materials are typically materials with complex crystal structures. Examples of such crystals can be seen in the paper "New and Old Concepts in Thermoelectric Materials" by Joseph Sootsman et al [6]. The complex structures tend to scatter phonons more easily, hence lowering the lattice thermal conductivity. However, the compound studied in this thesis, germanium telluride (GeTe), does not have a complex crystal structure, but rather a simple sodium-chloride configuration. Despite the simple structure, the lattice thermal conductivity of GeTe is low, making the question of why this is, interesting.

A possible explanation for the good thermoelectric properties of GeTe is that it experiences a structural phase transition between two very similar crystal structures. The lattice thermal conductivity of GeTe can be seen in the right plot in Figure 1.2. The lattice thermal conductivity for GeTe is the lowest just before the phase transition. Usually, when thinking about a phase transition it is the solid-liquid-gas transformations that first come to mind. This is known as a change of matter. On the other hand, the structural phase transition has no shift in the state of matter but rather modifies the lattice structure of the material. This means that the same compound might on a microscopical level have a different structure depending on parameters like temperature, pressure and composition [7].

The Free energy of the system decides whether the crystal structure of a compound changes or not. The structure with the lowest Free energy is the thermodynamically preferred structure. When one crystal structure gets lower Free energy than another possible structure, a phase transition can occur [7].

The phase transition occurring in GeTe is a first-order phase transition. This means that when the temperature approaches the phase transition, there is a sudden shift in the structural parameters and not a continuous transition. This can be seen in the left plot in Figure 1.2 for GeTe.

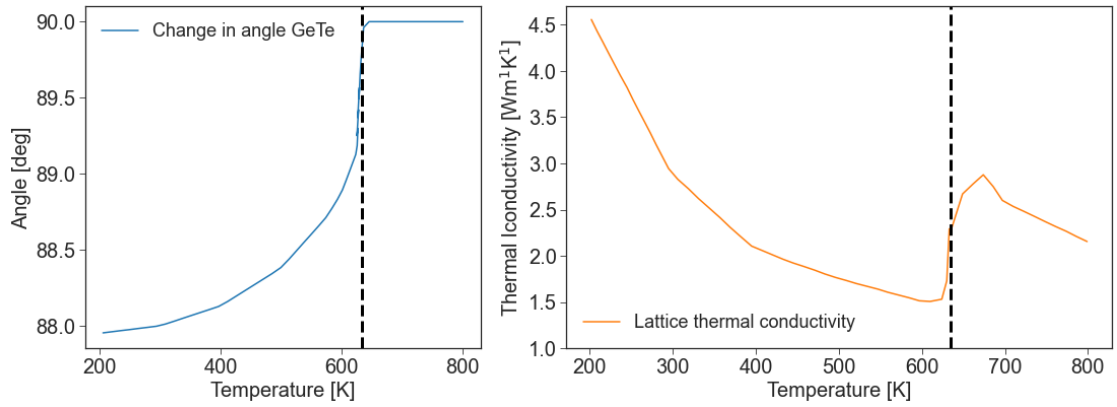

(a) (b)

Figure 1.2: GeTe as the (a) angle (b) lattice thermal conductivity changes as functions of temperature. The black solid lines represent the phase transition. The figures are adapted from [8, 9].

The aim of this master thesis is to investigate two competing phases of GeTe around the phase transition. The two phases are the trigonal and cubic structures as they have been experimentally found [10, 11]. The effects of the trigonal structure changing to be more cubic as the phase transition approaches will be also investigated. To make this investigation, the Free energy and phonon dispersion will be calculated using first-principles calculations with density functional theory (DFT) and temperature dependent effective potential (TDEP). Additionally, the effect of converging the force constants through an iterative approach will be explored. The phonon dispersion relation with and without broadening will be calculated in order to perhaps find a connection to why GeTe is a good thermoelectric material. Calculations will be made at various temperatures and trigonal unit cell angles in an attempt at finding and understanding the phase transition. The study's limitation is that thermal expansion caused by temperature changes will be omitted from the calculations, meaning the volume will be constant at the ground state size.

Chapter 2

Theory

In this chapter, a short introduction to GeTe will be made together with key concepts concerning crystals and lattice dynamics. This is to build a basis for understanding the phonon dispersion relation and the various effects that can occur surrounding phonons when dealing with a phase transition. In the last part of the chapter, the phase transition itself will be discussed.

2.1 Germanium Telluride

The focus of this thesis is on the investigation of the compound germanium telluride (GeTe). This is a material well known for its promising thermoelectric properties and phase-change abilities. GeTe has been found to have several solid phases. At room temperature, there are three possible states, amorphous-, rhombohedral- (α-GeTe) and orthorhombic-GeTe (γ-GeTe). At high temperatures, the crystal structure is cubic (β-GeTe) [12].

GeTe has a phase transition occurring at a temperature around $T = 630$ K ~ 740 K [8, 11, 13]. This transition happens between the rhombohedral structure and the cubic structure. The melting temperature of GeTe is at a temperature $T = 725$ °C $= 998$ K [14].

In addition to this, experiments have shown that GeTe has a low lattice thermal conductivity κ_{lat}. The trigonal structure has reported values around 2.7 $\text{Wm}^{-1}\text{K}^{-1}$ [15]. This low lattice thermal conductivity can perhaps be explained by the phase transition of GeTe and the lattice dynamics surrounding this.

2.2 Lattice dynamics

The study of the collective vibrations in a crystal is called lattice dynamics [16]. In order to understand the impact the phase transition has on the lattice, it is important to understand how the lattice behaves. Therefore, this section will present concepts regarding crystal structures, unit cells, and the direct and reciprocal lattice. Phonons and the dispersion relation will also be explained. This section is primarily based on the books "The Physics of Phonons" by Gyaneshwar P. Srivastava [5] and "Introduction to solid state physics" by Charles Kittel [17].

2.2.1 Crystal structure

In order to understand crystal vibrations, it is important to understand the crystal itself. An ideal crystal is made up of groups of atoms infinitely repeated in a periodic pattern. The repeating arrangement of these groups of atoms is called a crystal structure. This repeating unit can be defined as a unit cell. With suitable translational vectors repeating the unit cell, the cell can fill all space. All information about a crystal is contained within a unit cell.

Out of the unit cells, the smallest cell contains only one lattice point and is called a primitive unit cell, or a primitive cell. The primitive unit cell volume is spanned by the lattice vectors $\boldsymbol{a_1}$, $\boldsymbol{a_2}$ and $\boldsymbol{a_3}$. A face-centered cubic (FCC) primitive cell for the GeTe is illustrated in Figure 2.1a. Though the unit cell only has one lattice point, the cell can contain several atoms or molecules belonging to that single point. This group of atoms or molecules is called a basis. In Figure 2.1a the basis is one germanium and one tellurium atom. If the lattice point is at the centre of the germanium atom, they together form the primitive unit cell.

Though a primitive cell contains all the necessary information to build a crystal structure, it oftentimes might be more convenient to describe the crystal in a unit cell containing more atoms. One such cell is the conventional unit cell. Unlike the primitive cell, the conventional cell can have more than one lattice point. This can often make it easier to understand and visualise the crystal. An example of a conventional unit cell for a FCC structure containing 2 types of atoms can be seen in Figure 2.1b. The conventional cell of GeTe shows how the atoms are aligned in the same way as for rock-salt, NaCl.

The atom positions in a cell and the lattice vectors that define the cell volume are collectively called a supercell, as defined by David Sholl [7]. This means that both the conventional and primitive unit cells are supercells as long as they fulfil these requirements. When doing calculations on materials, information about the supercell is one of the most important inputs to give [7]. Depending on what calculations to make, the size of the supercell matters. A supercell consisting of four conventional unit cells can be viewed in Figure 2.1c.

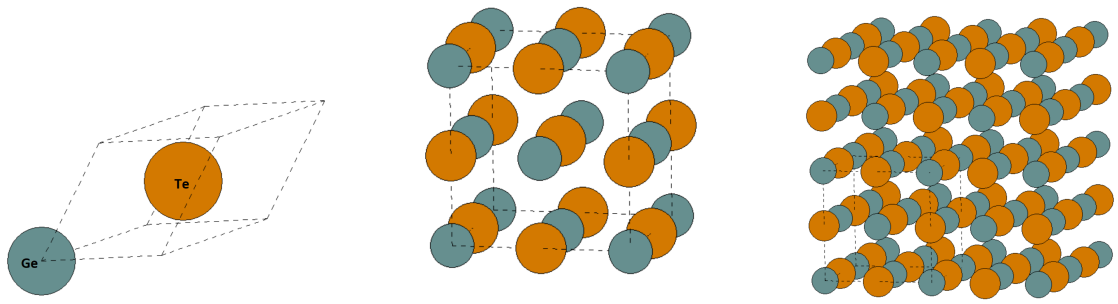

(a) (b) (c)

Figure 2.1: Three possible ways of representing the face-centered cubic (FCC) structure of germanium telluride (GeTe). The unit cells are (a) a primitive cell, (b) a conventional cell and (c) a supercell. The supercell in (c) contains 4 conventional cells.

There are several different ways the atoms can arrange themselves to create lattices. In order to sort the possible crystal lattices they are divided into 14 different lattices, called the Bravais lattice. These lattices can then be sorted into 7 different crystal systems, describing the shape of the unit cells.

The crystal structures discussed in this thesis are the cubic (face-centered cubic) and trigonal (rhombohedral) phases of GeTe. The lattice constants, the angles between the lattice vectors and the space group of the trigonal and cubic structure can be found in Table 2.1.

Table 2.1: The characteristics of the cubic and trigonal unit cells [18].

Crystal system	Cubic (β-Gete)	Trigonal (α-GeTe)
Bravais lattice	Face-centered cubic	Rhombohedral
Angles	$\alpha = \beta = \gamma = 90°$	$\alpha = \beta = \gamma \neq 90°$
Lattice constants	a=b=c	a=b=c
Space group	$Fm\bar{3}m$	$R3m$

As seen in Table 2.1 the difference between the cubic and trigonal cell shapes lies in the angle. This shift in the angle from the non-cubic to the cubic 90° results in the cubic being one of the structures with the most symmetry, while the trigonal structure has less so. The shift in angle also results in the shape of the trigonal structure being very similar to the cubic structure, only elongated in the [1 1 1] direction [19]. This is why the trigonal phase of GeTe is often called a quasi-cubic structure.

Another way that the structures can differ is by the atomic placement inside the unit cells. One unit cell shape can stay the same, but the atoms might position themselves in such a way that they are at a local or global minimum. At the thermodynamically most stable atomic positions, the atoms are at a global minimum.

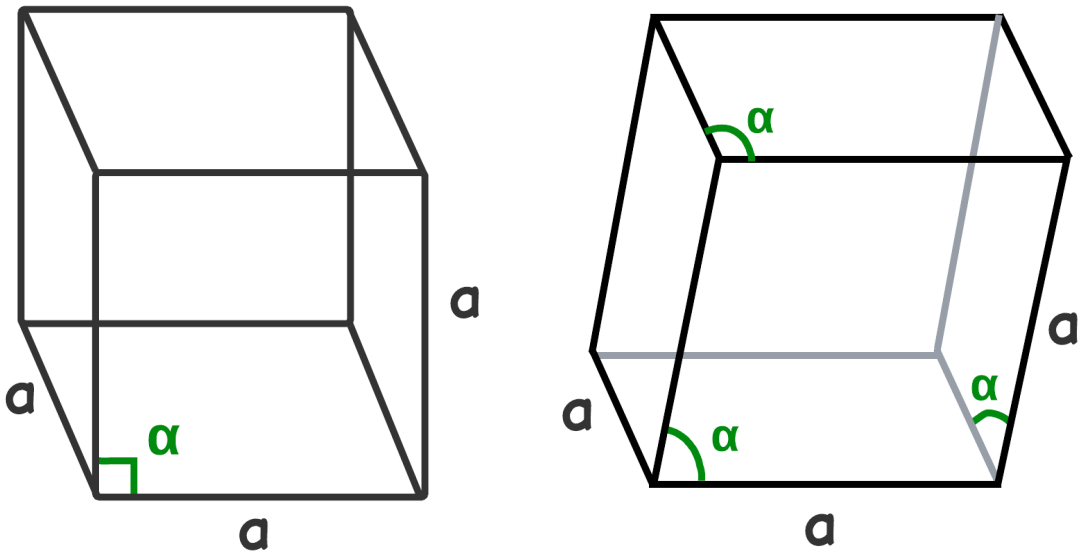

(a) Cubic unit cell

(b) Trigonal unit cell

Figure 2.2: The (a) cubic and (b) trigonal conventional unit cell geometries, with α and a being the angle and lattice constant respectively.

In Table 2.1 the space group for the two phases of GeTe have been listed. A space group is

defined by a series of symmetry operations that the structure can undergo, without having to change the positions of the atoms within the cell [20].

2.2.2 The direct and reciprocal lattice

Crystals have two associated lattices, the direct lattice and the reciprocal lattice. The direct lattice space is the three-dimensional space where each lattice point represents a basis. The lattice space is spanned by the lattice vectors, $\boldsymbol{a_1}$, $\boldsymbol{a_2}$ and $\boldsymbol{a_3}$. The vectors are defined so that the crystal arrangement looks the same at a point $\boldsymbol{r}$ as at a point $\boldsymbol{r'} = \boldsymbol{r} + u_1\boldsymbol{a_1} + u_2\boldsymbol{a_2} + u_3\boldsymbol{a_3}$, where u_i are arbitrary integers. The vector from a chosen point to another point in the lattice is described by the translation vector

$$\boldsymbol{T} = n_1\boldsymbol{a_1} + n_2\boldsymbol{a_2} + n_3\boldsymbol{a_3}. \tag{2.1}$$

Where n_j are integers. The dimension of the direct lattice vector $\boldsymbol{T}$ is in [length].

A mathematical representation of the crystal planes in the form of a lattice is often used when discussing crystals. This is the second associated lattice, the lattice in the reciprocal space. Every plane in the real space becomes a lattice point in the reciprocal space [21]. When mapping between the direct and reciprocal lattice the relationship

$$e^{i\boldsymbol{G}\cdot\boldsymbol{T}} = 1 \tag{2.2}$$

is used. Here $\boldsymbol{G}$ is the reciprocal translation vector, similar to the translation vector $\boldsymbol{T}$, only for reciprocal space.

The connection between the direct and reciprocal space can be mathematically described by the following equations

$$\boldsymbol{b_1} = 2\pi\frac{\boldsymbol{a_2}\times\boldsymbol{a_3}}{V_{cell}}, \quad \boldsymbol{b_2} = 2\pi\frac{\boldsymbol{a_3}\times\boldsymbol{a_1}}{V_{cell}}, \quad \boldsymbol{b_3} = 2\pi\frac{\boldsymbol{a_1}\times\boldsymbol{a_2}}{V_{cell}}. \tag{2.3}$$

Here $\boldsymbol{b_1}$, $\boldsymbol{b_2}$ and $\boldsymbol{b_3}$ are the reciprocal lattice vectors and $V_{cell} = \boldsymbol{a_1}\cdot\boldsymbol{a_2}\times\boldsymbol{a_3}$ is the volume of the unit cell. The reciprocal translation lattice vector is defined as

$$\boldsymbol{G} = m_1\boldsymbol{b_1} + m_2\boldsymbol{b_2} + m_3\boldsymbol{b_3} \tag{2.4}$$

with m_i being integer numbers. The dimension $\boldsymbol{G}$ is [1/length].

Brillouin zone

A primitive unit cell in the reciprocal space containing only one lattice point is called the first Brillouin zone. Depending on the crystal lattice and its symmetry, the Brillouin zone differs. The Brillouin zone for a FCC structure is shown in Figure 2.3.

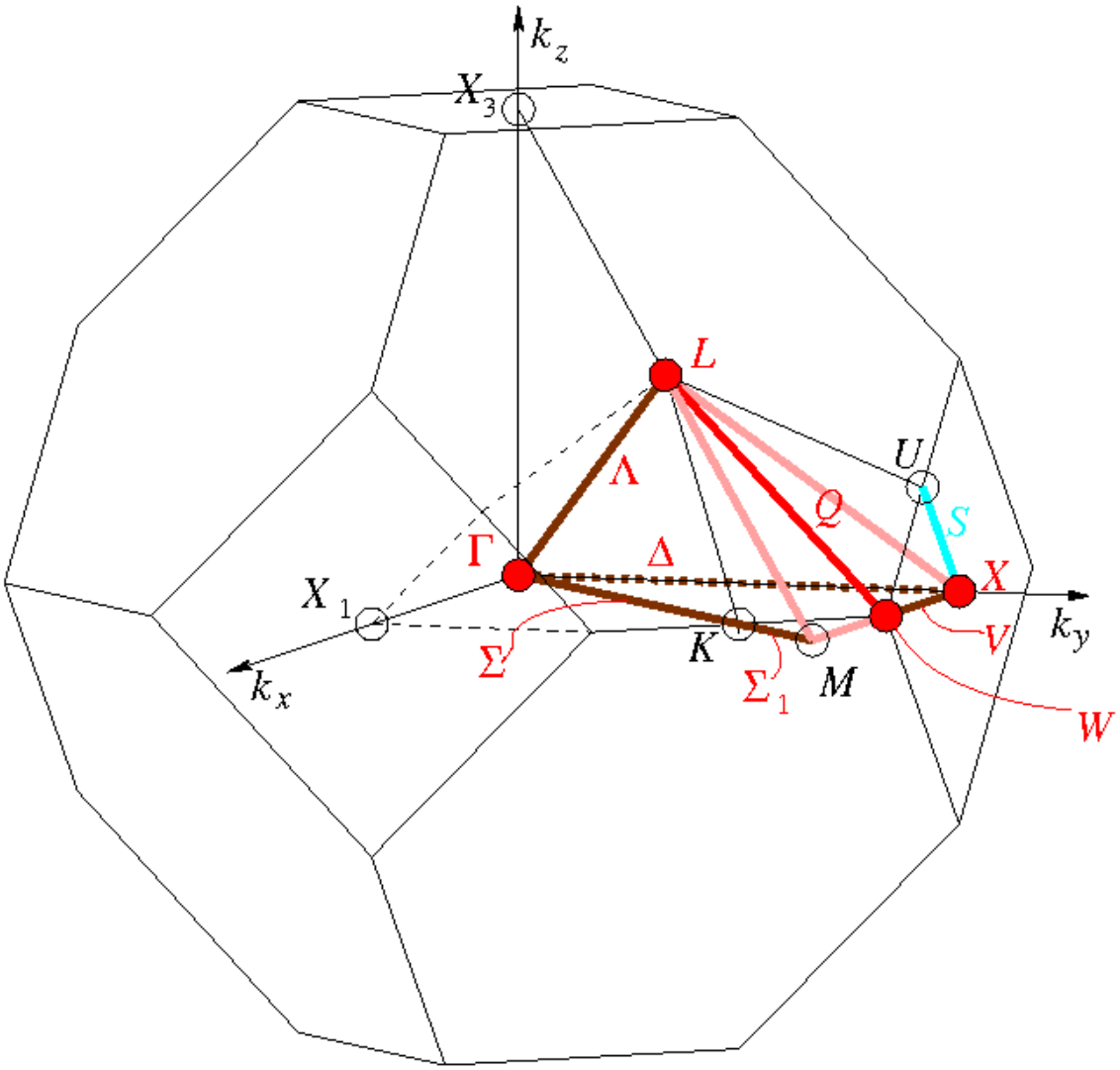

Figure 2.3: The Brillouin zone of the cubic phase of GeTe with symmetry group $Fm\bar{3}m$. The high symmetry points are marked with filled and unfilled circles. The figure is adapted from the Bilbao Crystallographic Server [22, 23].

It is very costly to sample the entire Brillouin zone when doing calculations. Calculations along lines between high symmetry points in the Brillouin zone are therefore usually made. The Brillouin zone for a FCC structure together with high symmetry points are shown in Figure 2.3. At the centre of the Brillouin zone, lies the Γ-point, the origin of the reciprocal space.

2.2.3 Phonons

Heat travels through a material by the collective vibrating atoms in a crystal known as phonons. The centre of mass for the atoms is stationary, but the relative motion of the atoms creates a wave effect and this is the phonons. For practical purposes, one assigns a momentum $\hbar\boldsymbol{q}$ to the phonons, with $\boldsymbol{q}$ being the wave vector. This particle-like behaviour of the atoms is called a quasi-particle.

Phonon dispersion relation

The phonon dispersion relation is the relationship between the energy (frequency, ω) and wave vector ($\boldsymbol{q}$). The relationship $\omega = \omega(\boldsymbol{q})$ is used for understanding phonons.

In a crystal with p atoms per unit cell, the displacement of the bth atom in the lth unit cell is denoted $u(lb)$. A Taylor expansion of the potential energy U is then as follows:

$$\begin{aligned} U = U_0 + \sum_{lb} \alpha \frac{\partial U}{\partial u_\alpha(lb)}\Big|_0 u_\alpha(lb) + \frac{1}{2!}\sum_{lb,l'b'}\sum_{\alpha\beta}\frac{\partial^2 U}{\partial u_\alpha(lb)\partial u_\beta(l'b')}\Big|_0 u_\alpha(lb)u_\beta(l'b') \\ + \frac{1}{3!}\sum_{lb,l'b',l''b''}\sum_{\alpha\beta\gamma}\frac{\partial^3 U}{\partial u_\alpha(lb)\partial u_\beta(l'b')\partial u_\gamma(l''b'')}\Big|_0 u_\alpha(lb)u_\beta(l'b')u_\gamma(l''b'') + ... \end{aligned} \tag{2.5}$$

$$U = U_0 + U_1 + U_2 + ... \tag{2.6}$$

Here U_0 is the equilibrium potential, and $\Phi_{\alpha\beta} = \frac{\partial^2 U}{\partial^2 u_\alpha \partial u_\beta}\Big|_0$ and $\Phi_{\alpha\beta\gamma} = \frac{\partial^3 U}{\partial u_\alpha \partial u_\beta \partial u_\gamma}\Big|_0$ are the second-and third-order force constants. α, β and γ are indices for Cartesian directions.

The first term in equation 2.5 can be set to zero in dynamic problems as it is the displacement of the atoms that are important. The second term in the equation disappears in the equilibrium configuration. The following equation represents the harmonic approach used for calculating the dispersion relation:

$$U_{\text{harm}} = U_2 = \frac{1}{2}\sum_{\alpha\beta}\sum_{lb;l'b'}\Phi_{\alpha\beta}(lb;l'b')u_\alpha(lb)u_\beta(l'b'). \tag{2.7}$$

To exemplify the phonon dispersion relation, one can look at an infinitely long diatomic system on a linear chain. This is illustrated in Figure 2.4. There are $2N$ atoms forming N unit cells and each unit cell has a length of $2a$. The m and M are the masses for the atoms in the cell with $m < M$.

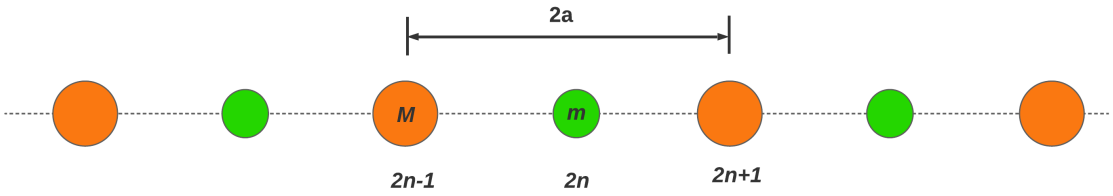

Figure 2.4: A diatomic linear chain. The masses m and M are alternating, with $m < M$. $2a$ is the length of the unit cell.

When one atom is moved away from its equilibrium position, the neighbouring atoms will "feel" this movement. This is approximated with there being a spring in between the atoms, making the atoms feel spring forces. This is in accordance with Hooke's law. The use of Newton's second law results in the equations of motion

$$m\frac{\mathrm{d}^2 u_{2n}}{\mathrm{d}t^2} = C[u'_{2n+1} + u'_{2n-1} - 2u_{2n}] \tag{2.8}$$

$$M\frac{\mathrm{d}^2 u'_{2n+1}}{\mathrm{d}t^2} = C[u_{2n+2} + u_{2n} - 2u'_{2n+1}] \tag{2.9}$$

for the atoms. Here C is the force constant and u_i is the displacement of atom i. The suggested solution for the displacements are

$$u_{2n} = A_1 e^{i(2nqa-\omega t)} \tag{2.10}$$

$$u'_{2n+1} = A_2 e^{i[(2n+1)qa-\omega t]} \tag{2.11}$$

with $\boldsymbol{q}$ being the wave vector and ω the frequency. Combining equation 2.8 and 2.9 with the equations of motion gives

$$-\omega^2 m A_1 = C[A_2 e^{iqa} + A_2 e^{-iqa} - 2A_1] \tag{2.12}$$

$$-\omega^2 M A_2 = C[A_1 e^{-iqa} + A_1 e^{iqa} - 2A_2]. \tag{2.13}$$

The solution to the two equations above can be expressed only if the determinant of the unknown coefficients A_1 and A_2 dissipates. By doing so one gets an expression for the phonon dispersion relation for a diatomic linear system

$$\omega^2 = C\Big(\frac{1}{m} + \frac{1}{M}\Big) \pm C\Big[\Big(\frac{1}{m} + \frac{1}{M}\Big)^2 - \frac{4}{mM}\sin qa^2\Big]^{1/2}. \tag{2.14}$$

Equation 2.14 is shown in Figure 2.5. The two signs in the equation indicate that there are two phonon branches or phonon modes. The two modes are the acoustic and the optical modes.

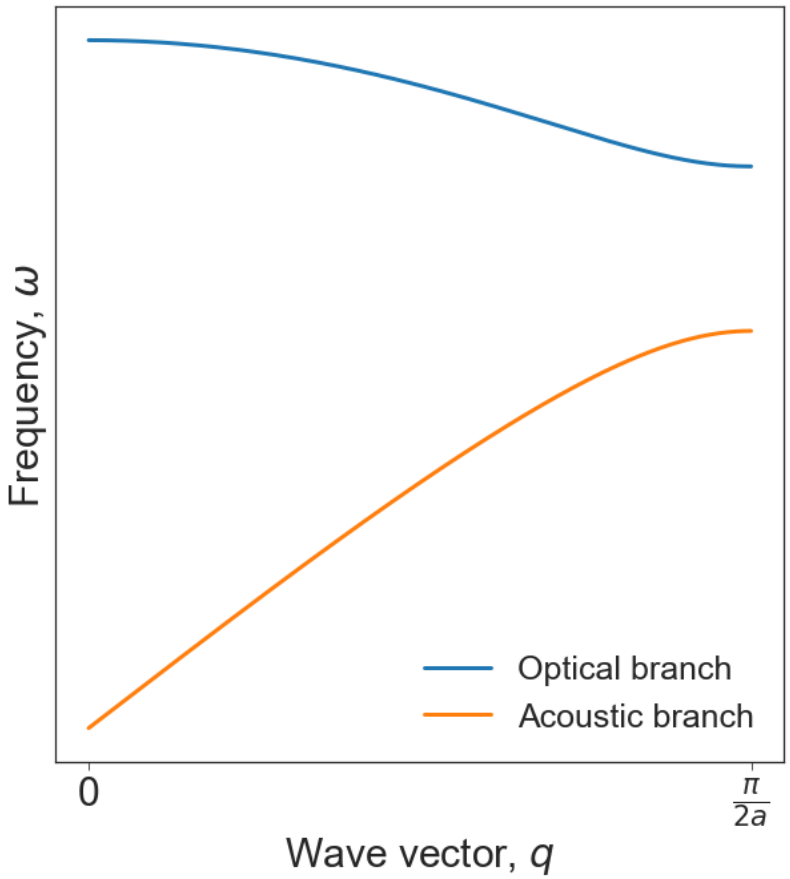

Figure 2.5: The dispersion relation for a diatomic linear lattice showing the optical and acoustical branches. The lattice constant is of length $2a$.

Although the diatomic linear chain is a simple system, it can still give information about a three-dimensional system. The number of phonon modes is determined by the number of

atoms in the unit cell. In the three-dimensional system with p number of atoms in the unit cell, there are a total of $3p$ phonon modes. There are three acoustic modes and $3p-3$ optical modes. In a diatomic system, there are three acoustic modes and three optical modes.

The modes can further be divided into longitudinal and transverse modes. This gives longitudinal LA and transverse acoustical TA modes, and longitudinal LO and transverse optical TO modes.

The phonon is acoustic when the atoms in the unit cell are vibrating together in phase. This is the same as sound waves through a material. The acoustic branches also have the property that $\omega(\boldsymbol{q}) \to 0$ when $\boldsymbol{q} \to 0$. This is at the Γ-point. The orange line in Figure 2.5 illustrates this for the diatomic linear chain.

Phonons out of phase within the unit cell are called optical phonons. They are named optical phonons because if the atoms are carrying opposite charges, they may excite a motion similar to the electric field of a light wave [17]. For optical phonons, $\omega(\boldsymbol{q}) \to$ constant when $\boldsymbol{q} \to 0$. This is visualised by the blue lines in Figure 2.5.

The Debye temperature

There is an upper limit to the frequency that the lattice vibrations can have. Using the Debye model, this limit is known as the Debye frequency (ω_D) and separates when the lattice vibration goes from collective to individual vibrations [24]. The temperature associated with this phenomenon is called the Debye temperature (θ_D) and is defined as

$$\theta_D = \frac{\hbar\omega_D}{k_B} \tag{2.15}$$

with $\hbar$ being the reduced Planck constant and k_B Boltzmann constant [17].

Lattice thermal conductivity

A reason to investigate phonons is their connection to the lattice thermal conductivity κ. κ describes how heat propagates through a material. The lifetime τ, heat capacity c and group velocity v of the phonons are connected to κ through

$$\kappa_{\alpha\beta} = \frac{1}{V}\sum_{\lambda} c_\lambda v_{\alpha\lambda} v_{\beta\lambda} \tau_{\beta\lambda}. \tag{2.16}$$

Here V is the volume, λ indicates the phonon modes and α and β are directions. For the high-symmetry cubic system equation 2.16 becomes

$$\kappa = \frac{1}{V}\sum_{\lambda} c_\lambda v_\lambda^2 \tau_\lambda. \tag{2.17}$$

From these equations one can see that the lattice thermal conductivity is dependent on how long the phonons live, the speed they travel and the heat they carry. The easiest property to observe in a phonon dispersion relation is the group velocity of the phonons. The group velocity $v = \frac{\partial\omega}{\partial q}$ can be seen in the dispersion relation as the slope of the branches. This means that the steeper the slope is, the higher the velocity.

The heat capacity is the property that converts energy to temperature. The heat capacity is closely connected to the Debye temperature and is at low temperatures obeying the T^3 law. This can be elaborated further in the Debye model, but will not be further

discussed here.

In the harmonic approach, the phonons act without interaction meaning they technically propagate infinitely. In order to include scattering effects, and hence lifetimes, the third-order force constants need to be included in the potential energy. This is called anharmonicity. What this entails will be discussed next.

At low temperatures the displacement of the atoms caused by the vibrating atoms, compared to the interatomic distances, is small and the phonons can be described using a harmonic potential. When the temperature increases the anharmonicity of the phonons increases, meaning the potential is no longer harmonic and the atoms can vibrate with larger displacements [25]. When the distances of the atoms are changing, so do the allowed energy states for the phonons. The phonons become less stable. This is visualised by a less well-defined phonon mode, called broadening. More broadening means that the phonon lifetime τ is shorter, something positive when wanting low lattice thermal conductivity as seen in equation 2.16. Broadening for trigonal GeTe can be seen in Figure 2.6.

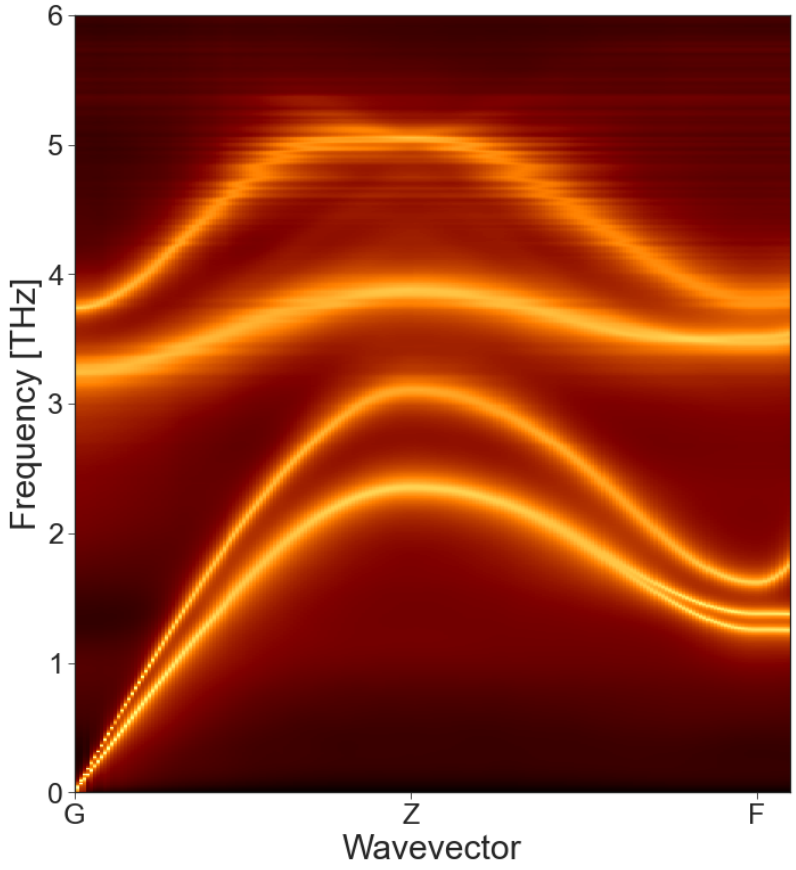

Figure 2.6: Dispersion relation of trigonal GeTe with broadening at $T = 700$ K.

Phonon softening

The frequency of a phonon mode can change when the temperature changes. If the frequency of the phonon modes decreases, this is called phonon softening. If a phonon softens all the way to a frequency of zero, the system is dynamically unstable.

If a structure has soft phonon branches (lower frequency) at low temperatures, the phonons might become more highly exited at higher temperatures. With more highly exited phonons,

the entropy of the system increases. This lowers the Free energy and can lead to a phase transition [17]. An example of phonon softening for the cubic phase of GeTe can be seen in Figure 2.7.

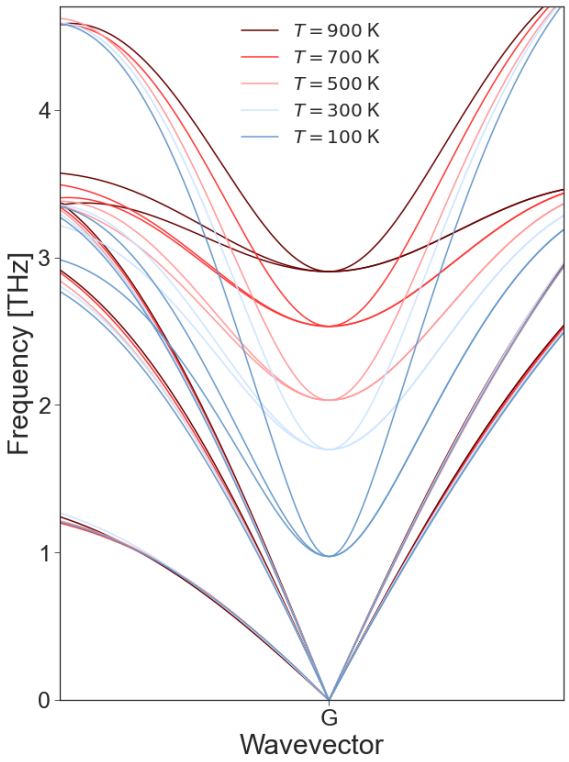

Figure 2.7: Phonon softening around the Γ-point for cubic GeTe.

Phonon softening can occur in the crystal lattice when a phase transition is approached. This can happen when approaching the transition both from above and below. In the first-order phase transition, discussed in the next section, the phase transition occurs before the phonon modes are able to reach zero [26].

2.3 Phase transition

The change of atomic arrangement in a crystal due to temperature change, called a structural phase transition, will be discussed in this section. The section will explain why a phase transition occurs in materials in addition to the distinction between the first- and second-order phase transitions.

2.3.1 Free energy

The reason why a ball rests at the bottom of a bowl instead of hanging on the edges is that it seeks the energetically lowest point to rest. The same principle applies to crystals and their atomic arrangements. Atoms try to stack themselves in the most stable and energetically lowest configuration. A quantity that can be minimised in order to find a phase transition is Free energy.

One way of calculating the Free energy is by Helmholtz's Free energy (F)

$$F(T) = U_0 - TS. \tag{2.18}$$

Where U_0 is the internal energy, while T and S are the temperature and entropy respectively.

A structure having the lowest Free energy at some conditions does not always mean being the most stable structure. The Free energy changes as the conditions change, and the difference in Free energy between structures changes at different rates. It is necessary to look at the difference in Free energy to see which state is the most stable. This gives the equation

$$\Delta F = \Delta U_0 - T\Delta S. \tag{2.19}$$

The temperature when a phase transition happens is called the critical temperature (T_c). At this temperature two competing structures A and B will have the same Free energy, $F_A(T_c) = F_B(T_c)$. Figure 2.8 shows the difference in Free energy between the two structures A and B as the temperature rises. Equation 2.19 was used in order to visualise the phase transition.

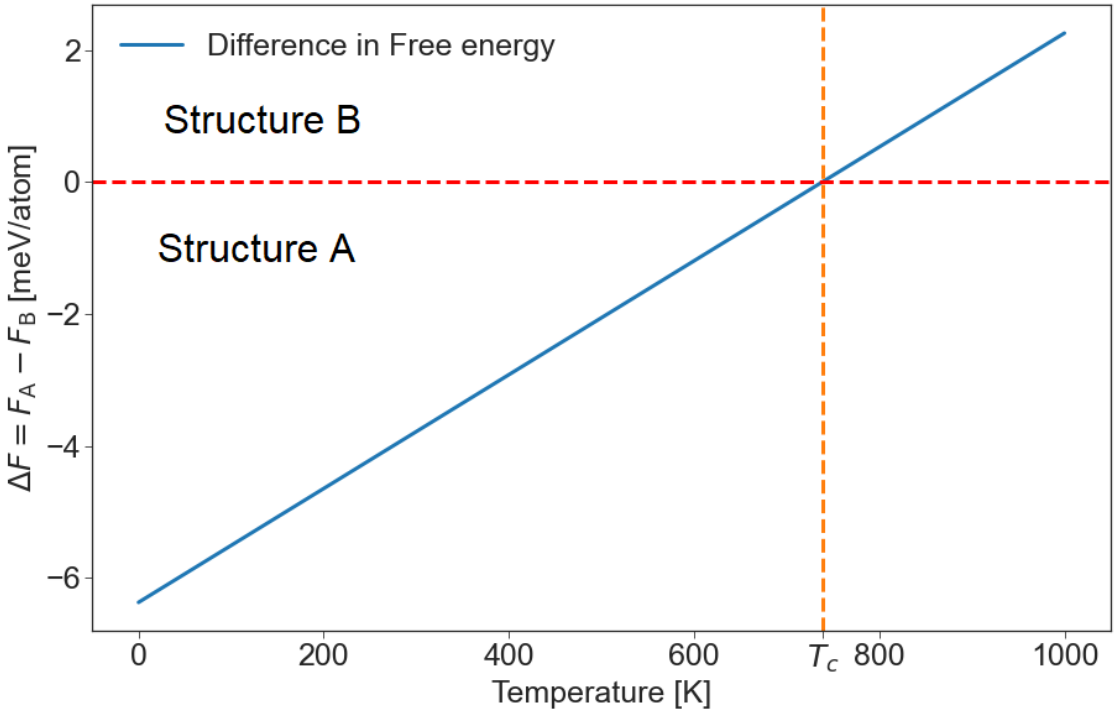

Figure 2.8: Phase transition is visualised by the difference in Helmholtz Free energy between structure A and structure B. Under the red dashed line, structure A is the most stable, and over the red line structure, B is the most stable state. In the intersection between the red and the blue line, a phase transition occurs at the critical temperature T_c.

2.3.2 First-and second-order phase transition

There are two different types of phase transitions, first-order and second-order. An order parameter, such as the distortion of a material μ, is used to see whether it is a first-order or second-order phase transition. During a first-order phase transition, there is a sudden shift in the order parameter when reaching the critical temperature. The order parameter

changes continuously in a second-order phase transition [27]. The first- and second-order phase transition is shown in Figure 2.9.

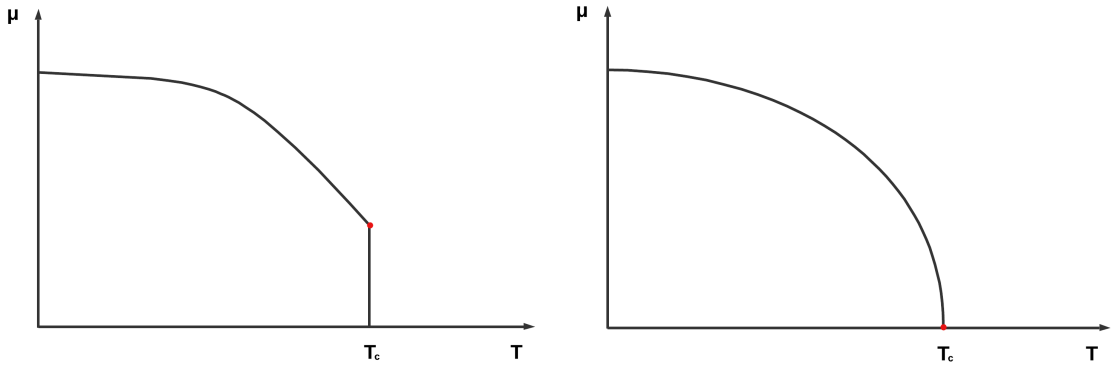

(a) First-order phase transition

(b) Second-order phase transition

Figure 2.9: Illustration of a (a) first-order phase transition and a (b) second-order phase transition as the temperature changes. The figure is adapted from [28].

Chapter 3

Computational methods

In this chapter, the methods used for doing ab initio calculations will be presented. This includes an introduction to density functional theory (DFT) and temperature dependent effective potential (TDEP). Furthermore, the iterative method of converging force constants will be discussed. A description of the calculations made in this study and their limitations on them will also be presented. Lastly, the convergence and choice of the numerical parameters used for the calculations will be presented together with the used software.

3.1 Density functional theory

The first principles calculations were made with density functional theory (DFT). DFT is an ab initio quantum mechanical modelling method that can be used for solving problems in chemistry, physics, materials science and more. It enables the user to find properties like the bandgap, total energy and density of states for a system [7]. This section gives an overview of the theory behind DFT and will not provide a comprehensive understanding of DFT. The following subsections will be based on a compendium by Clas Persson [29] and "Density Functional Theory a practical introduction" by David S. Sholl [7].

3.1.1 Kohn-Sham density functional theory

Schrödinger Equation

The description of particle behaviour is a subfield of physics called quantum mechanics and it is successful at predicting the behaviour of microscopic particles [30, 31]. In non-relativistic quantum mechanics, that describe particles and more complex systems like atoms and molecules, the fundamental equation is the Schrödinger equation (SE) [32]. The time-independent non-relativistic SE is given by

$$\hat{H}\Psi = E\Psi \tag{3.1}$$

Where $\hat{H}$ is the Hamiltonian operator, Ψ is the wave function and E is the energy of a system.

The state of a system is described by the wave function. In order to find the wave function the SE needs to be solved. As the shape of the wave function depends on the system, this can quickly become a challenging task.

For simple systems like the one-electron hydrogen atom, the SE can be solved analytically as there are few interactions to consider and it is possible to guess the solution for the wave function. In crystals, all interactions between the electrons, the electrons and nuclei and the nuclei themselves need to be considered. This makes the many-particle solution of the SE impossible to solve analytically.

In order to simplify the Schrödinger equation one can assume the motion of the electrons to be independent of the motion of the nuclei. The mass of the nuclei is much larger than the mass of the electrons and the positions of the nuclei can therefore be treated as fixed. This simplifies the SE so that the nuclei and the electron parts of the equation do not need to be solved simultaneously. This is called the Born-Oppenheimer approximation (BOA).

Hohenberg-Kohn theorems

To solve the SE, DFT makes calculations on atoms or molecules at the lowest possible energy state. This is called the ground state. This means that the systems that are calculated are at a temperature $T = 0$ K.

The two main theorems that DFT is based on are called the Hohenberg-Kohn theorems. The first theorem states that all ground state properties, like the ground state energy, are determined by the electron ground state density ($n(\boldsymbol{r})$) of that system. The density is given by

$$n(\boldsymbol{r}) = \sum_{j=1}^{N_e} |\psi_j^{\mathrm{KS}}(\boldsymbol{r})|^2 \tag{3.2}$$

where ψ_j^{KS} are single-particle auxiliary wave functions and N_e is the number of electrons in the system. The single particle wave functions are connected to the total wave function by a Hartree-like function $\Psi(\boldsymbol{r}_1, \boldsymbol{r}_2 ..., \boldsymbol{r}_{Ne}) = \psi_1^{KS}\psi_2^{KS}\psi_3^{KS}...\psi_{Ne}^{KS}$.

The second theorem states that if n_0 is the ground state electron density, n is another electron density and $E = E[n]$ is the energy density functional, then $E[n_0] < E[n]$. This means that when the energy density functional E is minimised, the resulting density for that minimisation is the ground state density n_0.

The form of the energy density functional is unfortunately unknown and because of the complexity of its nature, it might never be known. DFT is therefore incapable of finding material ground state properties on its own. However, by including the BOA and the Hartree-like wave function, the Kohn-Sham equation (KS-eq) can be expressed as

$$\Big\{ -\frac{\hbar^2\nabla_j^2}{2m_e} + V_H(\boldsymbol{r}) + V_{en}(\boldsymbol{r}) + V_{xc}(\boldsymbol{r}) \Big\} \psi_j^{KS}(\boldsymbol{r}) = \epsilon_j^{KS}\psi_j^{KS} \tag{3.3}$$

Here $\hbar$ is the reduced Planck constant and m_e the electron mass. The Coulomb repulsion between the electrons is described by the Hartree potential $V_H(\boldsymbol{r})$. $V_{en}(\boldsymbol{r})$ is the electron-nuclei interaction and $V_{xc}(\boldsymbol{r})$ is the exchange-correlation potential. Lastly, the Kohn-Sham eigenvalue of the jth electron is ϵ_j^{KS}.

While most of the terms in equation 3.3 are known, there are two terms that have no analytical solution. This is the exchange-correlation potential and the Hartree potential. In order for the KS-eq to be solved, the unknown terms need to be decided.

Exchange-correlation functional

There are several possible ways of approximating the exchange-correlation functional. The simplest approximated functional is the local density approach (LDA)-functional. This functional assumes that the exchange-correlation energy of the system is the same as in a uniform electron gas, meaning the electron density is constant; $n(\boldsymbol{r}) = \text{constant}$. The advantage of this is that the density of the electron gas is known and works as an approximation. Unfortunately, the LDA is incapable of accurately describing any other system other than the uniform electron gas.

There have been created several other exchange-correlation functionals that try to improve the LDA. A more complex functional is the generalised gradient approximation (GGA). Instead of a constant electron density, the GGA functional approximates the functional with a gradient $\nabla n(\boldsymbol{r})$. There are numerous different GGA functionals that include the gradient information in different ways, yielding different results.

In addition to the LDA and GGA, there have been created many other functionals. Which exchange-correlation functional yields the best results depends on the system, and needs to be tested. More complex functionals are more computationally expensive than simpler functionals which are important to consider when choosing functional.

Self-consistent calculations

The KS-eq have no analytical solution and therefore must be numerically solved. In addition to the exchange-correlation potential, the Hartree potential is also unknown. The Hartree potential needs the electron density, $n(\boldsymbol{r}) = \sum_j |\Psi_j^{KS}(\boldsymbol{r})|^2$, to be defined. The electron density is found by using the wave function, and the wave function is calculated by solving the KS-eq. Solving the KS-eq is therefore a self-iterative process and the steps to solve it are:

1. Choose an exchange-correlation functional.
2. Define an initial trial electron density $n(\boldsymbol{r})$.
3. Solve the KS-eq using the trial $n(\boldsymbol{r})$ to get the single-particle wave functions $\psi_i(\boldsymbol{r})$ and total energy.
4. Calculate the new electron density with equation 3.2.
5. Set the electron density to become the new trial electron density and start the process again from step 3.

The loop continues until the density is converged and ground state energy is reached. It is then possible to calculate the forces, elastic constants and ground state energy, that later will be used for calculations with temperature dependent effective potential.

3.2 Temperature dependent effective potential

Temperature dependent effective potential (TDEP) is a method that effectively extracts second-, third, and fourth-order force constants. At finite temperatures, it is a tool to calculate lattice dynamics such as phonon frequency, lattice thermal conductivity and Free energy [33]. TDEP can be utilised using results from any programme that is capable of calculating energies and forces from a given atomic configuration. Hence it is not a stand-alone programme but can be integrated with other programmes [33]. For this project, TDEP has been used together with DFT calculations in VASP to find the Free energy and

the phonon dispersion relation.

This section will give an understanding of TDEP. The text is based on the articles from Olle Hellman on TDEP [34, 35, 36] and the TDEP-manual website [33], that can be viewed for a deeper understanding of TDEP. The PhD theses by Rasmus A. Tranås [37] and Nina Shulumba [38], which both give an explanation of the TDEP method, have also been used.

3.2.1 Model Hamiltonian

As previously stated, DFT calculations are static calculations at the absolute zero temperature. In order for TDEP to extract second- and third-order force constants at finite temperature, TDEP finds a model Hamiltonian ($\hat{H}$) for the lattice dynamics. The expanded model Hamiltonian to the third order is given by

$$\hat{H} = U_0 + \sum_i \frac{P_i^2}{2m_i} + \frac{1}{2!}\sum_{ij}\sum_{\alpha\beta}\Phi_{ij}^{\alpha\beta}u_i^\alpha u_j^\beta + \frac{1}{3!}\sum_{ijk}\sum_{\alpha\beta\gamma}\Phi_{ijk}^{\alpha\beta\gamma}u_i^\alpha u_j^\beta u_k^\gamma. \tag{3.4}$$

Here $\Phi_{ij}^{\alpha\beta}$ and $\Phi_{ijk}^{\alpha\beta\gamma}$ are the second-and third-order force constants and u_i^α is the displacement from equilibrium for atom i in the direction α. The first two terms in the equation are the static lattice potential energy U_0 and the kinetic energy. The second-and third-order force constants represent two- and three-body atomic interactions.

In a two-body interaction, the second-order force constants can be represented in a matrix $\Phi_{ij}^{\alpha\beta}$ containing 3^2 variables. For a three-body interaction, the number of variables in the force constant matrix $\Phi_{ijk}^{\alpha\beta\gamma}$ is 3^3 [37]. The two- and three-body interactions are often referred to as harmonic and anharmonic force constants.

In crystals, there are an immense amount of force constants between the atoms. Some of these forces are similar to each other. In order to reduce the number of force constants that TDEP need to calculate, a series of symmetry operations can be applied to reduce the number of unknown variables. In addition to this, a cutoff radius r_c can be used to limit the distance where the two- and three-body interactions are considered.

From the model Hamiltonian the forces on atom i in direction α becomes

$$F_i^\alpha = \sum_{i\beta}\Phi_{ij}^{\alpha\beta}u_j^\beta + \frac{1}{2}\sum_{ij\beta\gamma}\Phi_{ijk}^{\alpha\beta\gamma}u_j^\beta u_k^\gamma. \tag{3.5}$$

The forces from all the atoms can be collected in the vector $\boldsymbol{F}_{\mathrm{TDEP}}$. The DFT calculated forces on the same set of atoms can be collected into the vector $\boldsymbol{F}_{\mathrm{DFT}}$. By making a comparison between the forces, TDEP minimises the difference between them,

$$\min_{\Phi}\Delta\boldsymbol{F} = \frac{1}{N_{\mathrm{TDEP}}}\sum_{i=1}^{N_{\mathrm{TDEP}}}|\boldsymbol{F}_{\mathrm{DFT}}^i - \boldsymbol{F}_{\mathrm{TDEP}}^i|^2. \tag{3.6}$$

Here N_{TDEP} is the number of configurations. After the minimisation, the model force constants can be used to calculate properties needing second-and third-order force constants. This includes the lattice thermal conductivity, Free energy and phonon dispersion relation, with and without broadening.

3.2.2 Free energy

The way that TDEP determines the Free energy of a system is by calculating the Helmholtz free energy [36]. Using the quasiharmonic approximation the Free energy is defined as

$$\begin{aligned} F &= U - TS \\ &= U_{\text{tot}} - TS_{\text{el}} + < E_k > + < U_{\text{vib}} > + U_{\text{zp}} - TS_{\text{vib}}. \end{aligned} \tag{3.7}$$

The electronic contribution, F_{el}, of the equation is divided into the total energy of the lattice, U_{tot}, and the electronic entropy, S_{el}. The rest of the terms are the kinetic energy E_{k}, the potential energy of the ions U_{vib}, vibrational entropy S_{vib} and the zero point energy U_{zp}, and are called the vibrational contribution, F_{vib}.

The electronic contribution is calculated from DFT calculations. The vibrational (phonon) Free energy can be calculated from statistical physics and is given by

$$\begin{aligned} F_{\text{vib}} &= -k_B T \ln Z \\ &= \sum_{\lambda} \frac{\hbar\omega_\lambda}{2} + k_B T \ln \Big[1 - \exp\Big(- \frac{\hbar\omega_\lambda}{k_b T} \Big) \Big] \end{aligned} \tag{3.8}$$

with k_B and $\hbar$ being the Boltzmann constant and reduced Planck constant. ω_λ is the frequency of the phonon mode λ and T is the temperature. Lastly, Z is the partition function for a harmonic oscillator [39]

$$Z = \prod_{\lambda} \frac{e^{-\beta\hbar\omega_\lambda/2}}{1 - e^{-\beta\hbar\omega_\lambda}} \tag{3.9}$$

where $\beta = \frac{1}{k_B T}$.

TDEP then combines the F_{vib} and F_{el} with an adjustment for a new baseline ΔU at a finite temperature and becomes the Free energy

$$F_{\text{TDEP}} = F_{\text{el}} + F_{\text{vib}} + \Delta U. \tag{3.10}$$

When doing calculations for the same supercell at different temperatures, the DFT calculations remain the same, and it is only the F_{vib} additions that change [33].

3.2.3 Canonical configurations

TDEP generates configurations of a supercell with slightly varied atomic positions to simulate the behaviour of atoms at a finite temperature. In this way, it captures the behaviour of a material at specific temperatures. Running DFT calculations on these configurations gives force constants and positions that can be extracted for further use. Figure 3.1 illustrates how three canonical configurations be created based on the input supercell (a).

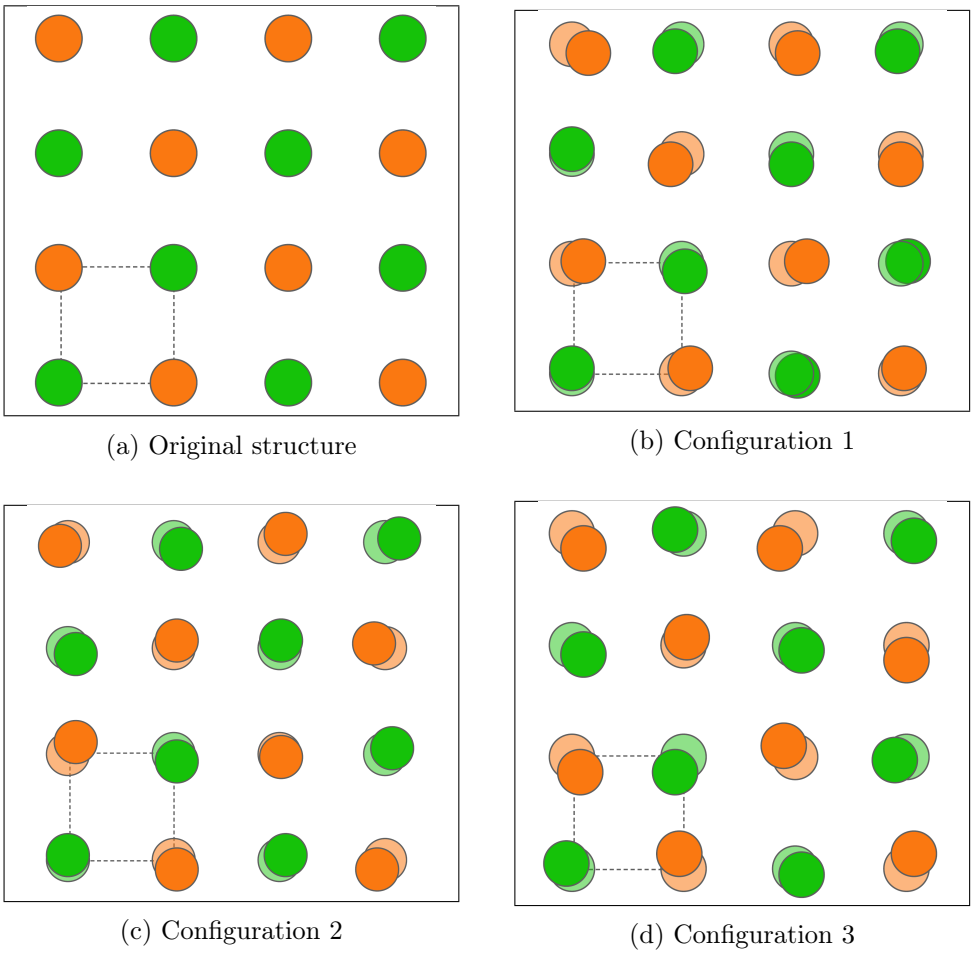

(a) Original structure

(b) Configuration 1

(c) Configuration 2

(d) Configuration 3

Figure 3.1: Visualisation of three different canonical configurations created from the input supercell in (a). The dashed square represents a unit cell. The different coloured circles are different atoms.

When creating canonical configurations in TDEP there are two options for doing this. One is to build the configurations from sets of force constants and positions. This requires that the user has available force constants and positions for their system. The other possibility is to use the Debye temperature to create approximated force constants for the canonical configurations. Calculated force constants for the crystal systems are better, but in the case where there are no force constants and position available, the Debye temperature approach can give a good result or starting point [40], though not for all types of calculations. Both of these approaches will be combined into an iterative method and used in this thesis.

To find the Debye temperature, the elastic constants for the cubic and trigonal phases of GeTe was calculated. The Debye model was then used to find the Debye temperature for the two phases from the elastic constants. The temperatures were $T = 238$ K for the trigonal structure and $T = 251$ K for the cubic structure. The Debye model is a model that estimates the phonon contribution to the specific heat in a solid [17]. For a more detailed explanation of the Debye method, please refer to the cited source.

3.2.4 Iterative process of finding force constants

When modelling phonons there is a need for high precision of the force constants. To get higher numerical precision, an iterative process has been used. As shown in Figure 3.2,

the first iteration is based on approximate force constants modelled from using the Debye temperature as explained in 3.2.3.

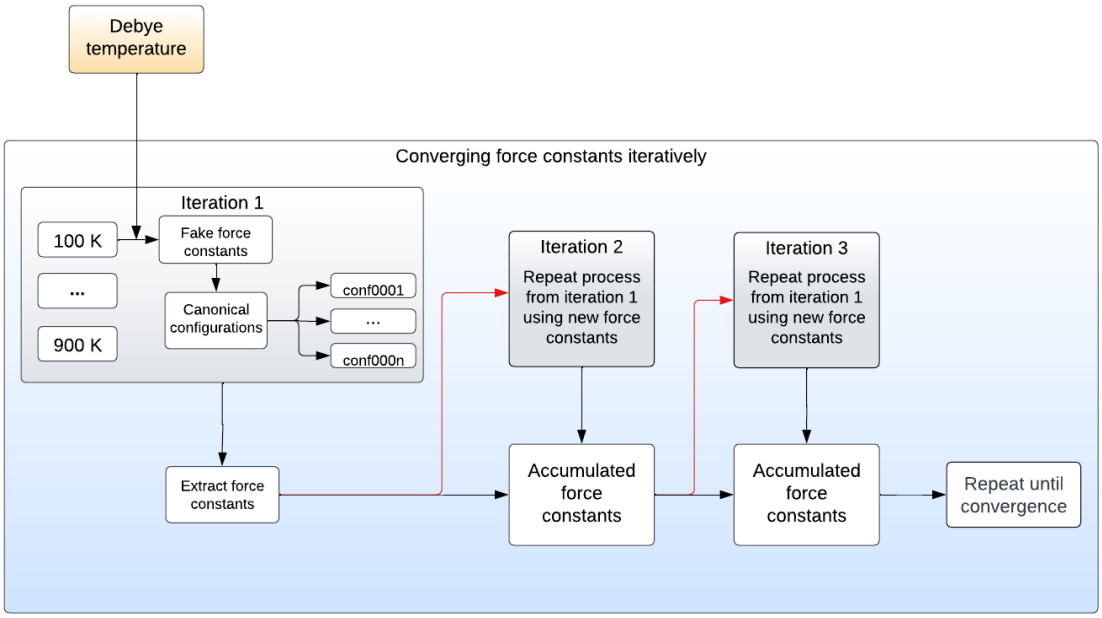

Figure 3.2: The iterative process of finding converged force constants. The first iteration of canonical configurations is built on fake force constants generated from the Debye temperature. The proceeding iterations are created based on the accumulated force constants from previous iterations. Each *conf000n* is a separate DFT calculation on the GeTe supercell.

The second iteration takes the extracted force constants from the first iteration and uses them to create canonical configurations. The third iteration extracts force constants from both the first and the second iterations. Using this iterative process, the TDEP model is provided with an increasing number of configurations to extract force constants from, where each iteration has higher precision than the last. The process continues until the force constants are converged. To see whether the force constants are converged or not, the difference in Free energy between two subsequent calculations has been checked. In this study, the achieved convergence was when the difference in Free energy was less than $\Delta F = 0.5$ meV/atom.

3.2.5 TDEP implementation

The steps for utilising the TDEP method are visualised in Figure 3.3 and Figure 3.2. The process can be summarised in the following steps:

1. Converge and relax a primitive unit cell.
2. Generate a supercell from the primitive cell with at least 100 atoms and as cubic shape as possible [33].
3. Generate n canonical configurations based on the Debye temperature and run individual DFT calculations on the configurations.
4. Extract forces corresponding to the positions of the various configurations.
5. Calculation of the second-order force constants.

6. Begin iterative calculations of force constants:
   (a) Generate n configurations from the accumulated previously calculated force constants.
   (b) Run DFT calculations for the new configurations.
   (c) Extract force constant and position pairs, from all previous iterations.
   (d) Calculate second-order force constants.
   (e) Repeat from 6a.
   When the change in Free energy between two subsequent iterations is sufficiently small, continue the process.
7. From the accumulated force constants, calculate temperature-dependent properties like the phonon dispersion relation, density of states (DOS) and Free energy.

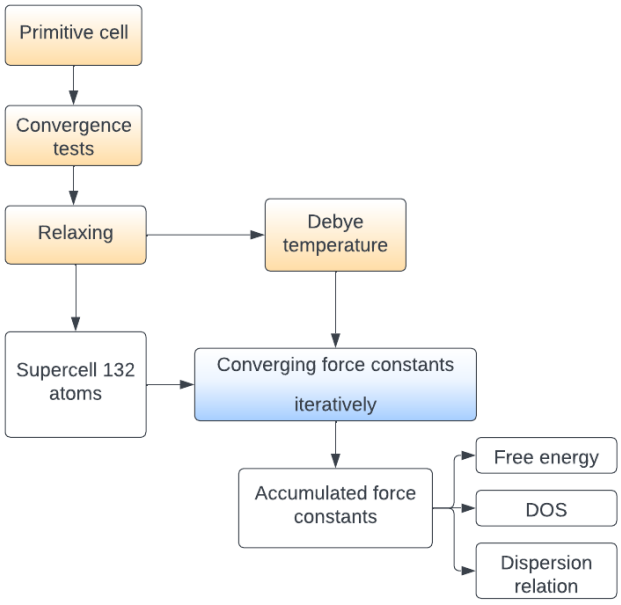

Figure 3.3: The process of using TDEP. A converged and relaxed primitive unit cell is used to find the Debye temperature. A supercell is created from repetitions of the primitive cell, before calculating force constants. After finding the force constants, lattice dynamics like the dispersion relation and Free energy can be calculated. The process of converging the force constants can be seen in Figure 3.2.

3.3 The calculations

In this section, the specifics of the calculations will be presented. This includes Free energy calculations, changing the angle for the trigonal structure and finding the phonon dispersion relation.

To investigate if a phase transition between the trigonal and the cubic phase of GeTe occurs, the Free energy for the phases was calculated at temperatures from $T = 100$ K to $T = 900$ K with an interval of 200 K. The Free energy was also calculated for the trigonal structure after having the cell shape changed to become more cubic. Angles ranging from

$\alpha = 88.6°$ to $\alpha = 90.4°$ with an interval of $0.3°$ was used. The Free energy at $90°$ was also included. This was done at 500 K, 600 K and 700 K. At every temperature and angle combination, the iterative process of finding force constants was used.

In order to change the angle of the trigonal unit cell, only the shape was changed and not the atomic positions with it. The trigonal cell was expanded from a primitive cell to a conventional quasi-cubic unit cell. It was the conventional unit cell that had its angle changed before the shape was cut down back to the primitive cell. The PYTHON script used for doing this can be found in Appendix A. After converging the force constants, the Free energy and phonons dispersion relation was calculated.

Limitations of the study

In order to get the full picture of the Free energy and phonon dispersion relation for the two phases calculations with various volumes, temperatures and angles (trigonal only) would be needed. Due to the time constraints of this thesis, some limitations were imposed in order to ensure timely completion. This includes the decision to keep the volume constant for all calculations except one.

In addition to this, some of the iterative processes for convergence of the force constants had to be stopped before reaching convergence. This was also due to time constraints.

3.4 Software

3.4.1 VASP and Atomic Simulation Environment

The Vienna *ab initio* Simulation Package (VASP) was used for the first-principles density functional theory calculations in this thesis. VASP can solve the Kohn-Sham equations and computes properties on the atomic scale from first-principles [41, 42, 43].

3.4.2 PYTHON packages

In order to change the angle of the trigonal primitive cell and find other properties like the distance and angles between atoms for the structures, the Atomic Simulation Environment (ASE) was used [44]. ASE is a tool written in the PYTHON programming language with easy integration with VASP.

Another PYTHON tool used is Scikit-learn. Scikit-learn is a tool much used in machine learning [45]. The function *r2_ score* has been used to calculate the R^2-score for fitted functions by using the formula

$$R^2(y, \hat{y}) = 1 - \frac{\sum_{i=1}^{n}(y_i - \hat{y}_i)^2}{\sum_{i=1}^{n}(y_i - \bar{y})^2} \tag{3.11}$$

Where $\bar{y}$ is the average value of the true calculations y_i, $\bar{y} = \frac{1}{n}\sum_{i=1}^{n} y_i$. $\hat{y}_i$ is the predicted value of the i-th calculation out of a total of n calculations.

3.5 Calculation details

3.5.1 Convergence tests

In order to solve the KS-eq, the DFT method needs a self-iterative process to reach self-consistency. To achieve this, there are some numerical parameters that need to be decided.

These are the energy cutoff, k-point density, pseudopotential and exchange-correlation functional. They all are parameters that can impact the numerical stability, precision and how computationally expensive the calculations are. For the TDEP method, the supercell size, force constants, number of q-points and the cutoff radius need to be decided.

Energy cutoff

In order to solve the KS-eq exactly, an infinite number of plane waves need to be summed over. This is not feasible to do for a computer and therefore an energy cutoff is introduced when calculating. The energy cutoff represents the highest energy that the plane waves can have when being summed over. Though not all possible plane waves are included, it is known that the high-energetic plane waves contribute relatively little to the shape of the wave functions [7].

When deciding the energy cutoff, DFT calculations for the primitive cells were made at energies ranging from 350 eV to 900 eV with intervals of 50 eV. The number of k-points for these calculations was $4 \times 4 \times 4$.

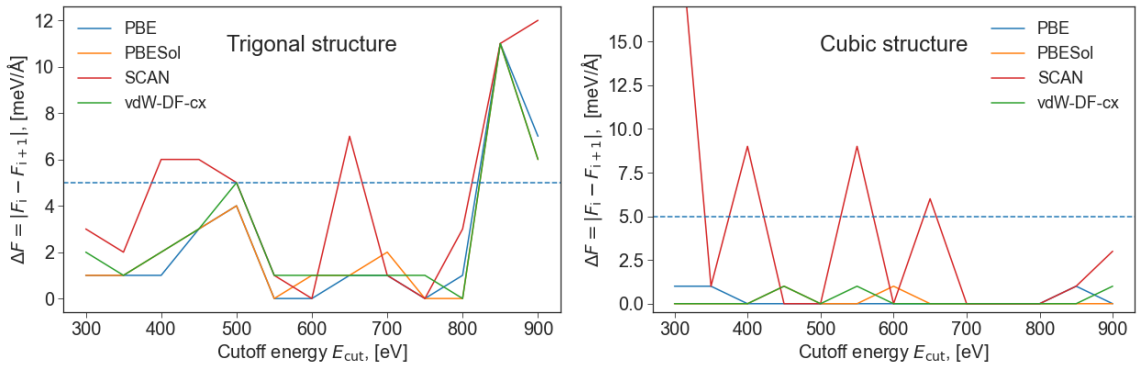

(a) (b)

Figure 3.4: Convergence tests of the forces for the functionals PBE, PBEsol, SCAN and vdW-DF-cx for the energy cutoff. Figure (a) and (b) is for the trigonal and cubic primitive cell respectively. The blue dashed line represents the convergence criterion for the forces at $F = 5$ meV/Å.

In Figure 3.4 the change in the largest interatomic force that the system is experiencing as the cutoff energy rises is plotted. For the trigonal unit cell, everything is relatively well converged until $E_{\text{cut}} = 850$ eV. The resulting energy cutoff for the calculations was set to 520 eV despite the sudden inaccuracy at $E_{cut} = 850$ eV.

The cutoff energy was set to 520 eV because of two reasons. One is that the computational cost increases with higher cutoff energy. When doing convergence tests on a small primitive cell with two atoms, the calculations are quick. When doing calculations on supercells with over 100 atoms a high cutoff energy will be too expensive.

The other reason for choosing 520 eV is that this cutoff energy matches the cutoff energy used for the calculations in "The Materials Project" [46]. In the early stages of the study, several functionals were considered. If the PBE functional was used, the values from this study could directly be compared to their values. In addition to this, it is recommended to use a cutoff of at least 30 % over the default cutoff value for the chosen pseudopotentials. 520 eV is the highest needed value for any pseudopotential in VASP

using this criterion.

K-point density

Another numerical parameter that needs to be tuned is the number of k-points used for calculating the DFT energies. At each k-point, a summation of an integral occurs. This makes choosing a suitable k-mesh important for the calculations not to be too computationally expensive. The chosen size for sampling k-points in this thesis is $10 \times 10 \times 10$ around the Γ-point for the primitive cells. This resulted in a k-point density of 6.5 around the Γ-point [47]. When this density was used for the 132 atoms supercell the mesh became $3 \times 3 \times 3$.

Pseudopotentials

The innermost electrons in an atom, known as core electrons, are usually not important when defining the physical characteristics of materials. It is the less tightly bound valence electrons that are important for these purposes. An approximation of a potential for the core electrons and the nucleus that matches the physical and mathematical properties of the true ion core is made. This is called a pseudopotential [7].

In VASP there are several different pseudopotential libraries available. The projector augmented wave (PAW) potentials [48] have been used as pseudopotentials and the specific potentials were Ge_d for germanium and Te for tellurium. Comparing the Ge_d and Ge pseudopotentials, the difference would be that Ge_d includes the electrons in the $3d^{10}$ band as valence electrons in the calculation and not as core electrons. The Ge pseudopotential has 4 valence electrons, the Ge_d pseudopotential has 14 and Te has 6.

Exchange-correlation functional

As previously mentioned, it is necessary to determine which exchange-correlation functional to use. The exchange-correlation functionals used for initial testing are the GGA functionals PBE [49] and PBEsol [50], the meta-GGA functional SCAN [51], and the van der Waals (vdW) functional vdW-DF-cx [52]. For the cubic primitive cell, except for the SCAN functional, all the functionals are converged, even at small energies as seen in Figure 3.4. The results will show that the vdW-DF-cx functional has been chosen as the final functional for the calculations.

Supercell size

In order to include enough information from the forces between the atoms, it is important to have a sufficiently large supercell. This is to be able to extract unique force constants to get precise phonon calculations. A bigger supercell means more atoms described explicitly. This again means that calculation will be more computationally expensive. A trade-off between the precision of the calculations and the supercell size needs to be made.

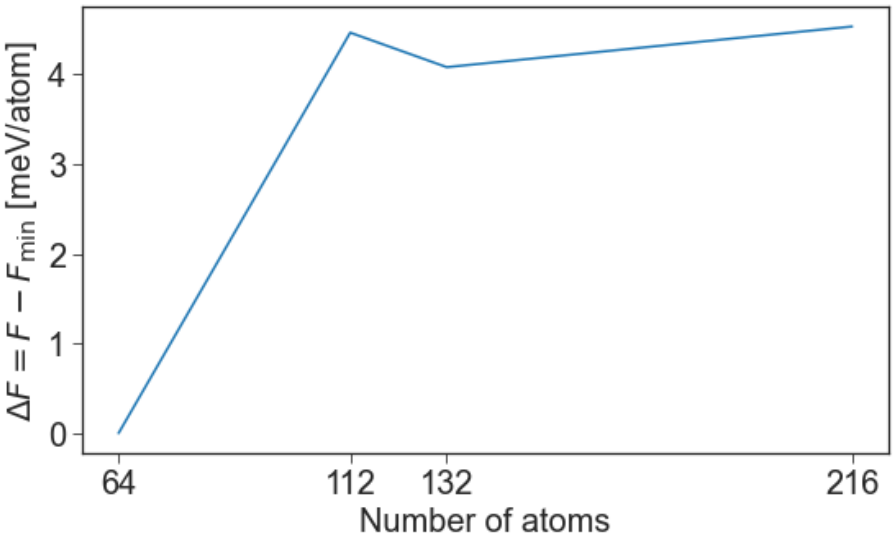

Figure 3.5: How the Free energy per atom for the trigonal supercell at 600 K changes with the number of atoms in the supercell.

In Figure 3.5 the Free energy for 4 trigonal supercells with different numbers of atoms is visualised. From 64-112 atoms there was a significant shift, after that, the energy stabilised. A supercell size of 132 atoms was therefore chosen since this supercell had a more cubic shape than the 112 atoms supercell.

Cutoff radius

One way to reduce the number of force constants that TDEP need to calculate, is by setting a cutoff radius to limit the sampling range. This has been explained in section 3.2.1. The effect of choosing different second-order force constant cutoff radii can be seen in Figure 3.6. When holding the third-order cutoff radius ($r_{c,3}$) constant and changing the second-order radius cutoff ($r_{c,2}$) the intensity state peaks change position. The intensity states are the number of energy states at a certain frequency. The chosen high symmetry point for the calculations was the L-point. The L-point in a FCC Brillouin zone can be seen in Figure 2.3.

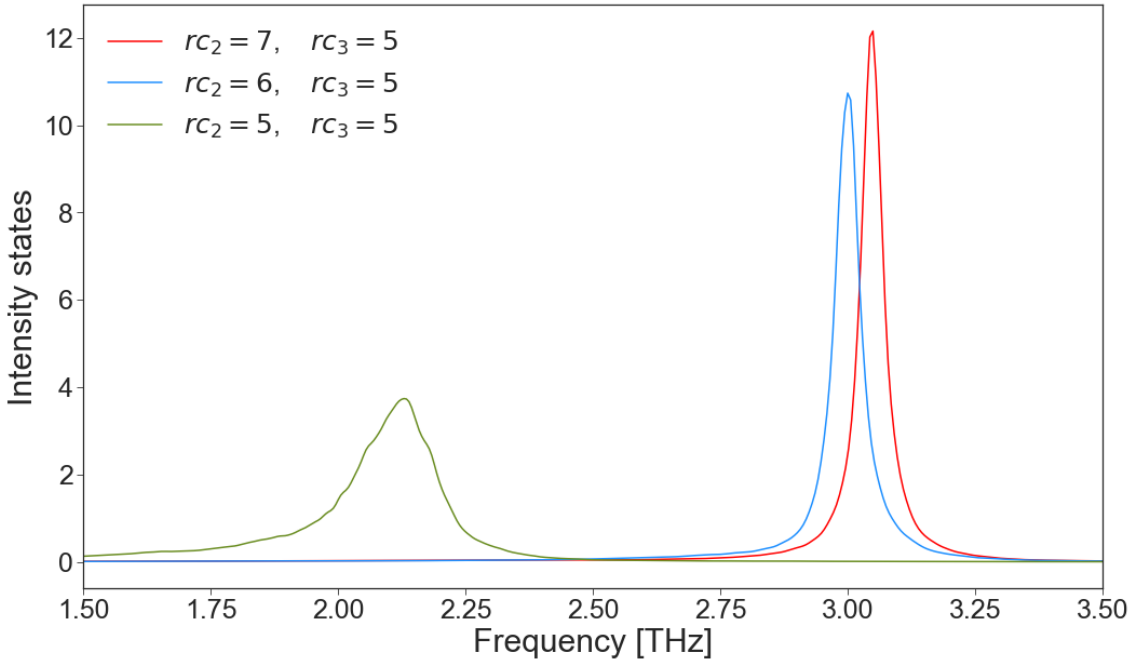

Figure 3.6: The intensity states of one mode at the high-symmetry point L for a constant third-order cutoff $r_{c,3} = 5$ Å and different second-order radius cutoffs.

There is a large shift from holding $r_{c,3} = 5$ Å to $r_{c,2} = 6$ Å, as seen in Figure 3.6. This indicates that the increase in radius includes atoms with sets of force constants and position pairs that provide more information.

When changing the cutoff radius for sampling atoms for the third-order force constants $r_{c,3}$, a shift in the intensity peak, between the radius $r_{c,3} = 5$ Å and $r_{c,3} = 6$ Å happens. This shift changes the height of the peak and not so much its position, which the second-order cutoff radius does.

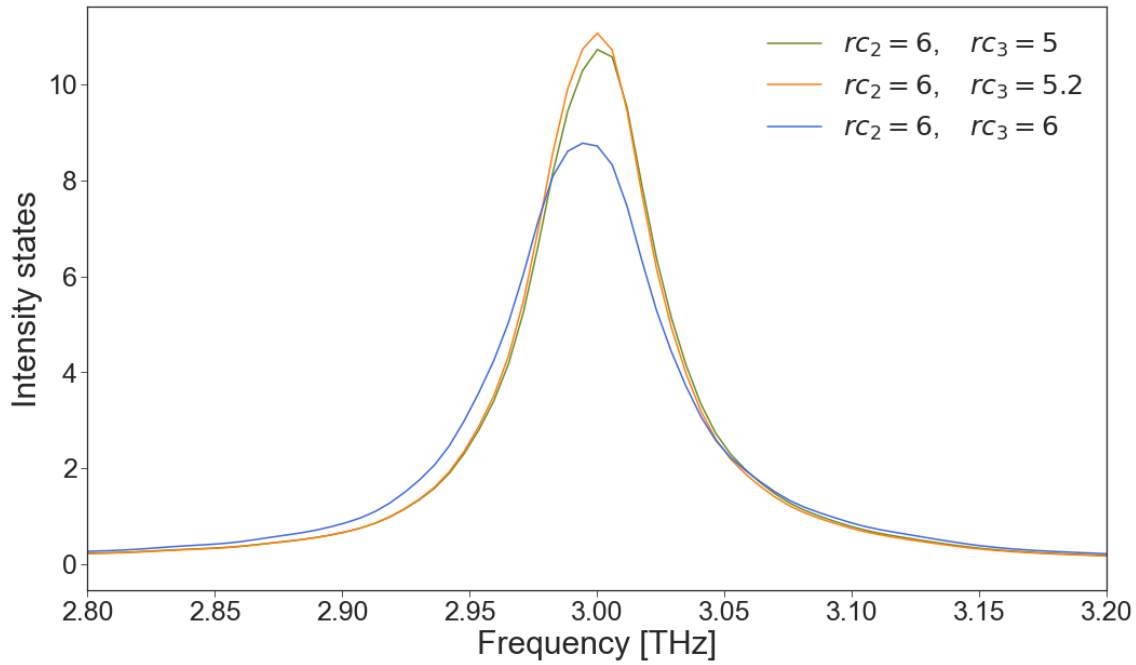

Figure 3.7: The intensity states for one mode at the high-symmetry point L when keeping $r_{c,2}$ constant and changing $r_{c,3}$.

From these results, the radius used for extracting the second-order force constants was the maximum for the 132-atom supercell. At the radius $r_{c,2} = 7.3$ Å this was achieved. The radius for the third-order cutoff radius was chosen to be $r_{c,3} = 5$ Å for the calculations to not be too computationally expensive. The number of included neighbours at different distances can be seen in Table 3.1.

Table 3.1: The number of neighbouring atoms at different cutoff radii r_c for the cubic structure.

Cutoff radius, r_c [Å]	Neighbours per atom
5.0	18
5.2	26
6.0	32
7.0	56
7.3	80

qg-point convergence

To get the phonon dispersion relation with smearing the number of **q**-points (denoted qg-points in TDEP) needs to be specified. The computational cost is rapidly rising with higher **q**-points, so it is important not to use excessively many.

The cubic structure at $T = 600$ K was used. To converge the q-points a high-symmetry point with much smearing was first chosen. For the cubic structure, the L-point was chosen. Convergence was tested with respect to the full width half maximum (FWHM) to see whether the width of the intensity peaks changed considerably when increasing the number of q-points. In addition, the change in positions of the peaks was also used to see

if enough q-points were included.

To find the FWHM and intensity peaks, the curves were fitted to a Lorenzian function [53] using the *curve_fit* function in the PYTHON package Scipy [54]. The resulting **q**-points became a $16 \times 16 \times 16$ grid.

Chapter 4

Results

The presented results have been found using the approach and tools described in Chapter 3. This includes calculations of the Free energy and dispersion relation for the trigonal and cubic phase of GeTe, with first and last iteration force constants. Calculations of the Free energy and phonon dispersion relation were made in order to find the phase transition and the effect the phonons might have on the lattice thermal conductivity in GeTe. The comparison between the first and last iteration of force constants is used to visualise the effect of using accumulated force constants from iteratively found force constants.

The vdW-DF-cx exchange-correlation functional and converged force constants are used for all calculations unless otherwise specified. This applies to all the results except in Section 4.1 where DFT ground-state calculations of primitive cells have been made.

4.1 Choice of functional and energy surface

In order to find which functional to use, ground state calculations where the cell shape, atomic positions and volume all could relax were made. An overview of the calculated structural parameters is presented in Table 4.1. This includes angle, volume and lattice constant, depending on the functional. The angles vary from $\alpha = 57.75° - 58.82°$ with the experimental average at $\bar{\alpha} = 57.95°$. The calculated volumes range from $V = 52.43$ Å^3 to $V = 59.12$ Å^3 with the experimental data having an average of $\bar{V} = 53.61$ Å^3.

Table 4.1: Calculated ground-state (0 K) and experimental structural parameters for the trigonal phase of GeTe. Four different GGA functionals and one vdW-DF functional were used for the calculations. The experimental data have been found at [10, 13, 55]

Functional	Primitive angle [deg]	Conventional angle [deg]	Volume [Å^3]	Lattice constant [Å]
PBE	57.75	88.01	56.23	4.377
PBEsol	58.82	88.97	52.43	4.240
revPBE	56.53	86.89	58.20	4.457
RPBE	56.53	86.89	59.12	4.496
vdW-DF-cx	58.67	88.83	53.20	4.265
Experimental results				
Wdowik (309 K) [10]	58.03	88.26	53.42	4.29
Goldak (300 K) [55]	57.94	88.14	53.87	4.31
Chattopadhyay (295 K)[13]	57.93	88.17	53.52	4.31

As discussed in Chapter 3, different functionals yield different results at equilibrium. Not only are the values of the ground-state energies different, but the shape of the cells might also differ. The results in Table 4.1 show how a number of functionals have relaxed the trigonal structure of GeTe differently, both over and underestimating the volume and angle. It is important to note that the calculated values are at 0 K, while the experimentally found angles are at room temperature. This means that the GeTe trigonal angle and volume at $T = 0$ K might be different and are not directly comparable.

The PBE functional has the best corresponding angle to the angles found experimentally, with a difference of $\Delta\alpha = 0.20°$. Comparing the experimentally found and calculated volumes, the PBE functional volume has a large difference of $\Delta V = 2.26$ Å^3, despite the correctness of the angle. Although this study is investigating the angle change of GeTe the difference in volume is large, resulting in the PBE functional not being chosen for this study.

The angle of the vdW-DF-cx functional is less similar to the experimentally obtained angles compared to the results obtained using the PBE functional. Regardless, the difference of $\Delta\alpha = 0.72°$ is not too large. The volume found by the vdW-DF-cx functional is considerably closer to the experimentally found values, with the difference being only $\Delta V = 0.41$ Å^3. The vdW-DF-cx functional was therefore chosen because of its likeness to the experimentally found trigonal structure structural parameters, in addition to including vdW interactions.

The calculations made in Figure 4.1 are DFT ground state calculations with varying angles and fixed volume showing the energy for different functionals. The figure shows how the functionals PBE, PBEsol and vdW-DF-cx give different energy minima at different angles, again emphasising their differences.

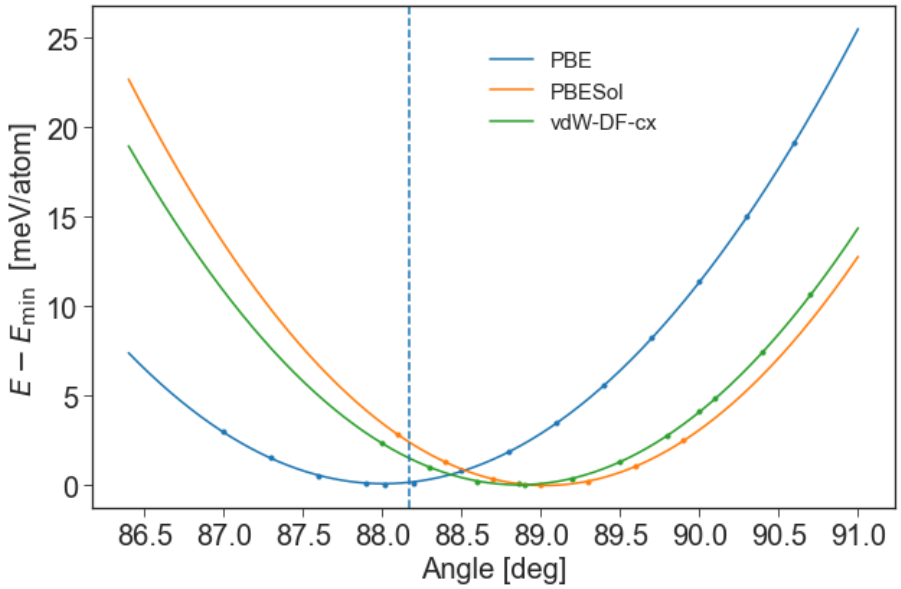

Figure 4.1: DFT calculations for the three functionals PBE, PBEsol and vdW-DF-cx with varying angles. The dashed line represents the experimentally found value for the angle at 300 K [13]. The angels are conventional cell angles.

In Figure 4.2 the energy landscape for the trigonal structure has been visualised. The red points in both subfigures show the energy minimum. This energy minimum is the same as that of the vdW-DF-cx functional (green) in Figure 4.1. The calculations were done by changing the lattice constant and angle systematically using a PYTHON script shown in Appendix A. After changing the cell shapes, the atomic positions inside the unit cells were relaxed using VASP while keeping the volume constant. Lastly, the energy was calculated.

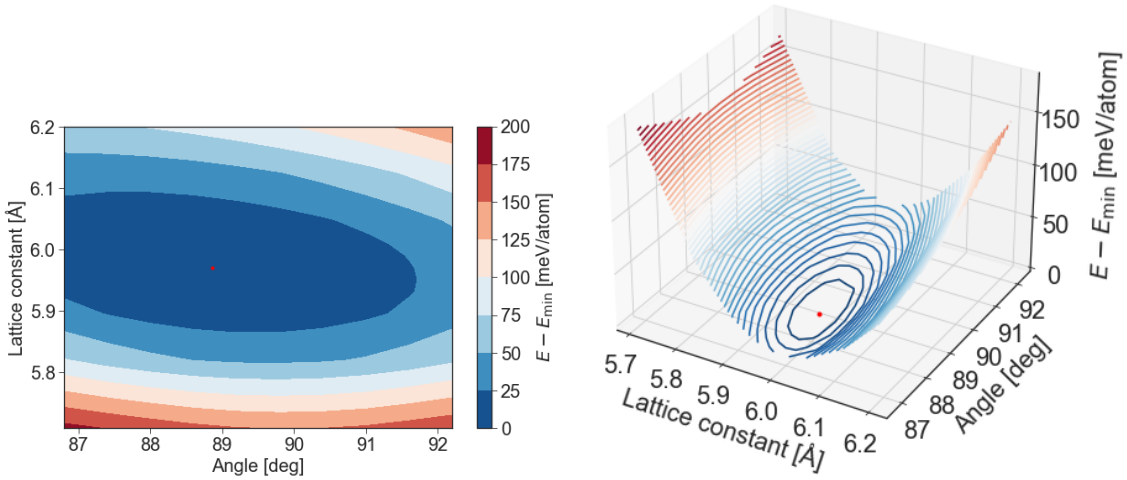

(a) (b)

Figure 4.2: Contour plot showing the energy landscape in 2D (a) and 3D (b) for trigonal GeTe at $T = 0$ K using the vdW-DF-cx functional. The angles and lattice constants are for the conventional unit cell.

The energies in Figure 4.2 are not mirrored around 90°. This is unexpected as the trigonal unit cell has the same cell shapes at $\alpha = 90° \pm n$, with n being an angle difference. The

distance between the germanium and tellurium atoms explains some of the reasons for the lack of symmetry. The shortest interatomic distances d listed in Table 4.2 shows that at $\alpha = 89.8°$ the distance between the atoms d is longer than at $\alpha = 90.2°$. This shows that there are unintentional inherent differences between the unit cells at $90° \pm n$.

Table 4.2: The shortest distances between the Ge and Te atoms in a selection of unit cells. The distances have been found using ASE.

Unit cell	Ge-Te distance [Å]
Trigonal relaxed 0 K	2.843
Trigonal 89.8°	2.856
Trigonal 90.0°	2.848
Trigonal 90.2°	2.849
Cubic relaxed 0 K	2.967
Cubic enlarged	2.985

To find the relationship between the volume and the angle, more calculations on the trigonal unit cell were made. While maintaining the volume of the trigonal unit cell at specific volumes, the shapes of the unit cells were relaxed. Doing so enabled finding the angle as a function of volume. This can be seen in Figure 4.3. As the volume decreases, the angle increases. The cell shape approaches a nearly cubic shape at a 12 % reduction of the volume of the fully relaxed trigonal unit cell (red line).

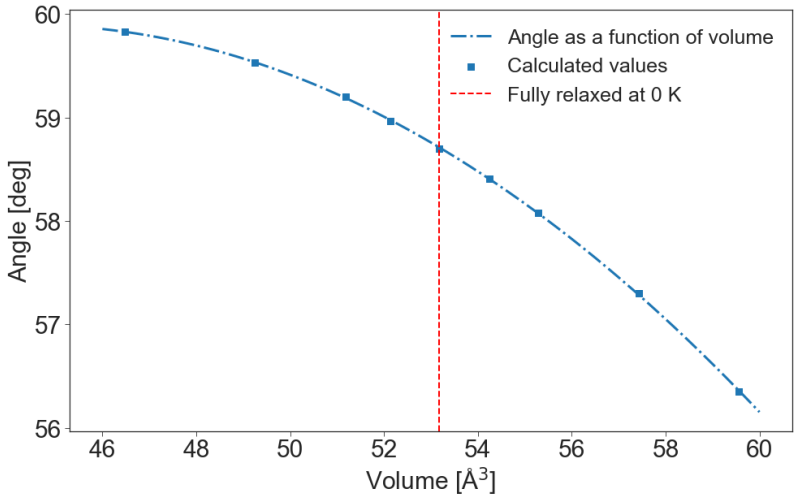

Figure 4.3: The preferred unit cell angle when relaxing the trigonal structure at $T = 0$ K while holding the volume fixed. The values for volume and angle are for the primitive unit cell.

4.2 Phase transition

In this section, an attempt at finding a phase transition between the trigonal and the cubic phase of GeTe was made. The reason for finding the phase transition is to later be able to closely investigate the phonons' behaviour around the critical temperature T_c. Results

from using one iteration force constants and the last iteration force constants will be presented. This is to visualise the effect of iteratively finding more accurate force constants. The iterative process of finding force constants has been explained in Section 3.2.4.

The supercells used for the remaining calculations contain 132 atoms, for both the trigonal and cubic structures. The Free energy has been calculated using equation 3.10. This means that a TDEP calculated contribution to the Free energy will be added to the DFT calculated ground state energy.

4.2.1 Temperature change

When attempting to find the phase transition in GeTe, the primitive unit cells used to create supercells have been fully relaxed at ground state. This means that all variables, volume, atomic positions and cell shape, have been relaxed. The resulting cell should be in the energetically lowest possible state at $T = 0$ K. When further doing calculations using the methods described in 3.2.5 at higher temperatures, the ground state unit cells were kept constant.

After one iteration of force constants, a critical temperature at $T_c = 740$ K was found, indicated by the orange line in Figure 4.4. The R^2-score, calculated by using scikit-learn and equation 3.11, was found to be $R^2 = 0.82$. Convergence of the force constants resulted in changes in the Free energy for the trigonal and cubic structures, causing the phase transition to vanish. The last iteration force constants resulted in the Free energy difference indicated by the blue line in Figure 4.4. The R^2-score was found to be $R^2 = 0.90$.

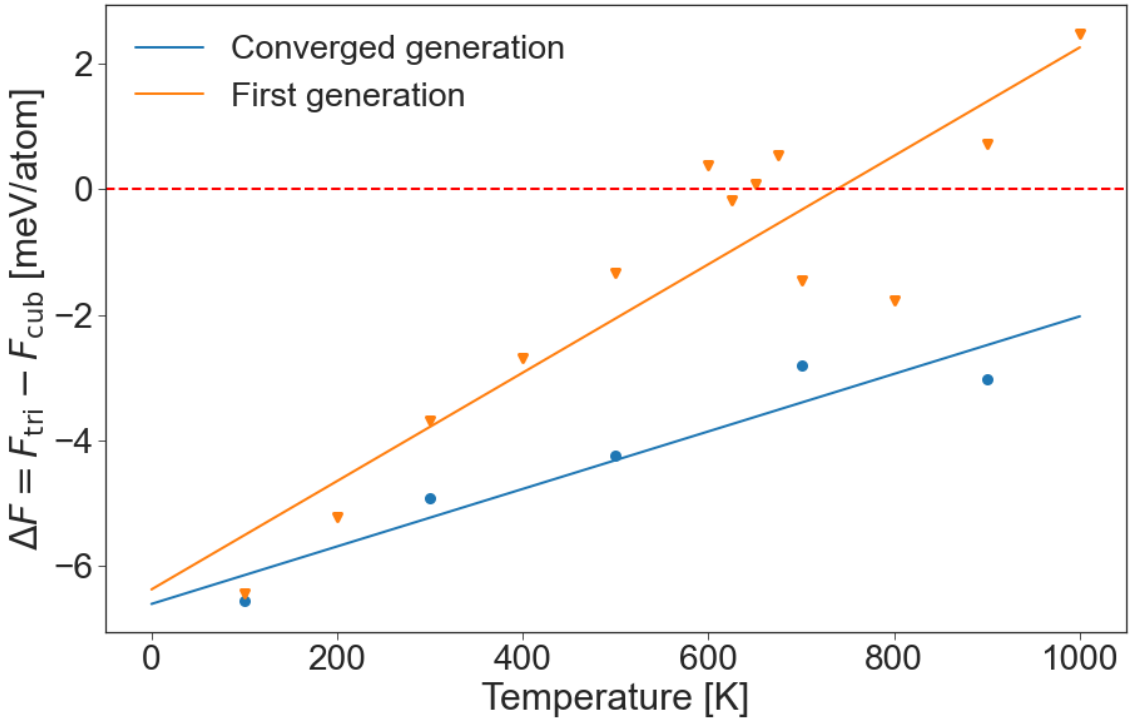

Figure 4.4: The difference in Free energy between the cubic and the trigonal structure. The orange points and line are the calculated values and the linearly fitted curve for the first iteration force constants. Similarly for the blue coloured line and points, but for the last iteration force constants. The area over the red line indicates a cubic phase, while the area under the line is the trigonal phase.

Figure 4.5 visualises the change in Free energy when adding more iterations of force constants. The calculations reached a convergence of $\Delta F = 0.5$ meV/atom. At a temperature $T = 900$ K the Free energy difference varies a lot even after seemingly having reached convergence. This is clearly shown by the cubic structure. Despite reaching convergence, the difference in Free energy for the temperatures $T = 500$ K and $T = 700$ K still exhibit variation. The calculations at the temperatures $T = 100$ K and $T = 300$ K vary substantially less as indicated by the blue lines. If calculations were to be made at only $T = 100$ K and $T = 300$ K, the convergence criteria could be much lower, making the calculations have higher precision.

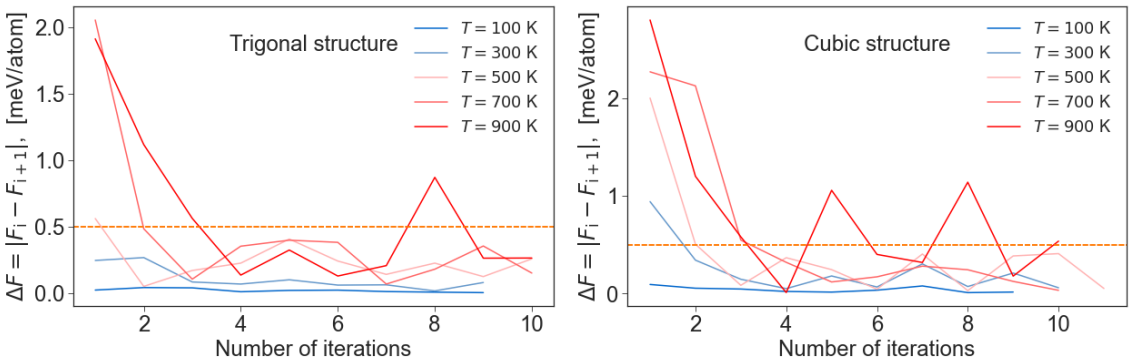

(a) (b)

Figure 4.5: The convergence of force constants for the (a) trigonal and (b) cubic structure at various temperatures. The convergence criterion $\Delta F = 0.5$ meV/atom is marked with an orange dashed line.

4.2.2 Angle change

When approaching the phase transition, studies have found that the trigonal angle goes toward $\alpha = 90°$, making the trigonal cell shape more cubic [13, 55]. To replicate the effect that the trigonal cell transitions to become more cubic, calculations of the trigonal cell with changes in the angle were made. In order to not change too many variables, making the search too extensive for this study, the lattice constant of the unit cells was chosen to be kept constant. This resulted in slight variations in the volumes as the trigonal structure changed angle. The trigonal volumes ranged from $V = 53.12$ Å^3 to 53.21 Å^3, with the fully relaxed trigonal cell at ground state having a volume of 53.18 Å^3. The calculated Free energies for the trigonal structure have been considered unaffected by these minor variations in volumes. The volume is therefore referred to as being constant throughout this study.

No phase change was found when initially calculating the Free energy. Therefore, the experimentally found critical temperature, at around $T = 630$ K ~ 740 K has been used as a reference. The Free energy has been calculated using various angles at $T = 500$ K, 600 K and 700 K, as described in Section 3.3.

The calculated Free energies at the three different temperatures can be viewed in Figure 4.6. The dashed lines represent a second-order polynomial fit to the calculated points at each temperature. The calculated Free energies show no tendency to follow the second-order polynomial trajectory, except for the $T = 600$ K calculations. The R^2-scores for the fitted curves at temperatures 700 K, 600 K and 500 K were respectively 0.23, 0.88 and 0.47. The range of R^2-scores indicates that the accuracy of the calculations is inadequate to draw clear conclusions about the phase transition due to an angle change.

At $T = 600$ K the R^2-score reached its maximum, while also having the highest amount of iterations and canonical configurations. In addition to this, the calculations at $T = 600$ K had the smallest difference in Free energy between the last two calculated iterations. The temperature with the lowest R^2-score is at $T = 700$ K. Fewer iterations were used to converge the force constants and there is a larger gap in the Free energy between the last two calculated iterations. The convergence plots associated with the force constants used in Figure 4.6 can be found in Appendix B.

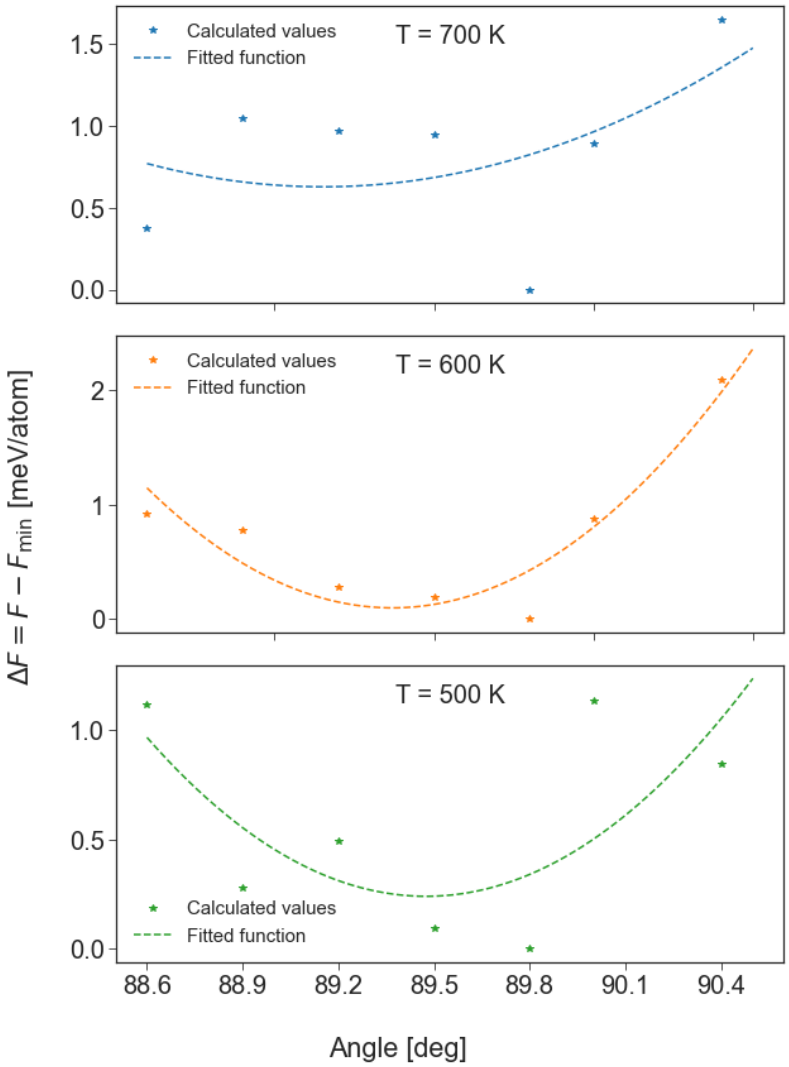

Figure 4.6: Calculated Free energy with a fitted curve at the temperatures $T = 500$ K, 600 K and 700 K over a range of angles.

When looking at the calculations made at $T = 600$ K, one can see that the energy minimum is at angle $\alpha = 89.37°$. This is a difference of $\Delta\alpha = 0.54°$ from ground state calculations indicating that when the temperature rises, the trigonal structure becomes more cubic.

4.2.3 Comparison at 700 K

Further investigation of the Free energy was made at $T = 700$ K in an attempt at discovering why the phase transition was not found. When changing the angle of the trigonal structure to $\alpha = 90°$, it is expected that the resulting cell is cubic. In order to compare the trigonal and cubic structures, to see whether they in fact are identical, a change to the cubic volume was made.

This resulted in one more calculation for the cubic structure being made at $T = 700$ K. The calculation was performed on an enlarged cubic cell. The larger cell has the same volume as the trigonal structure at $\alpha = 90°$, making direct comparisons of the Free energy and dispersion relations easier.

Figure 4.7 illustrates a comparison of all computations conducted for the trigonal and

cubic structures at $T = 700$ K. The Free energy from the fully relaxed trigonal structure (orange) serves as the baseline. The red points are the Free energies for the cubic structure and the blue points are for the trigonal structure with various angles.

The calculations at $T = 700$ K achieved a convergence of $\Delta F = 0.5$ meV/atom and are marked with error bars in Figure 4.7.

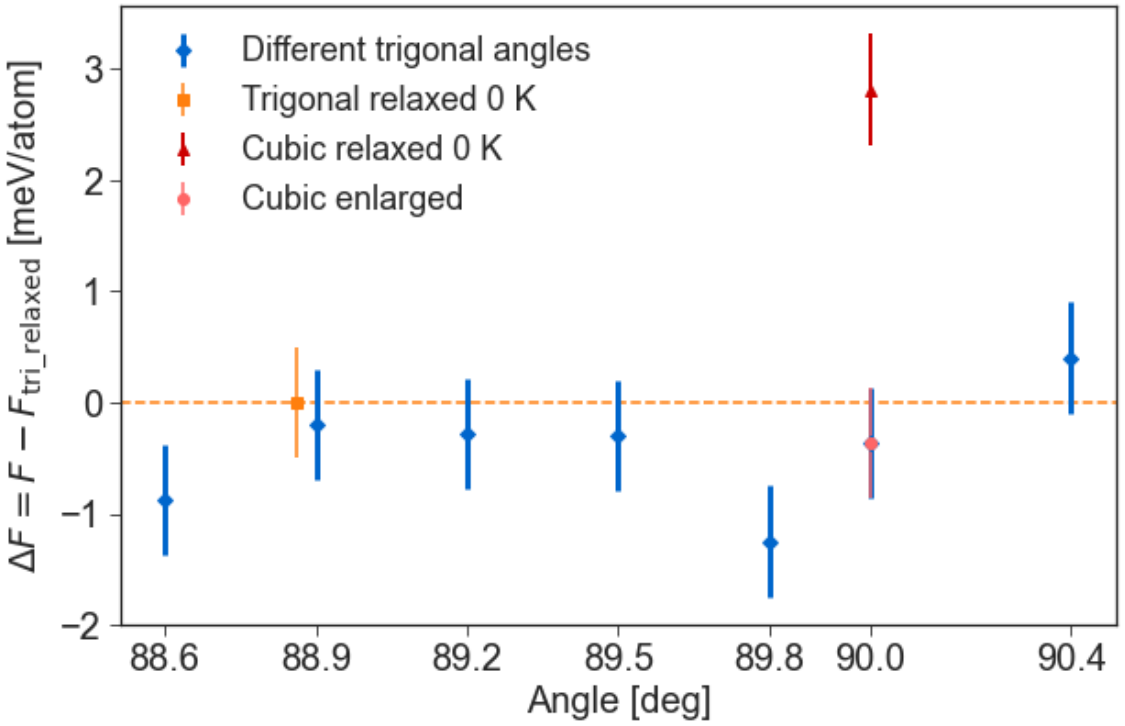

Figure 4.7: Comparison of the different calculated energies at 700 K. The calculations of the trigonal structures are all at constant volumes and are marked with blue points. The red marks are for the cubic structure with a fully relaxed primitive cell and a cell with the same volume as the trigonal cells. The fully relaxed trigonal structure with ground state structural parameters is used as the baseline.

From Figure 4.7 one can see that the calculated Free energies are all approximately the same. They all lie in a range of $F = 1.67$ meV/atom from each other, except the Free energy of the cubic structure with the ground state found volume.

Increasing the volume of the cubic cell has a significant effect. After changing the volume, the Free energy for the cubic structure dropped by $\Delta F = 3.17$ meV/atom becoming similar to the calculated Free energy for the trigonal structure at $\alpha = 90°$. This is a clear indication that the volume is important when calculating the Free energy, and therefore important when finding the phase transition.

4.3 Phonon dispersion relation

The dispersion relations for the cubic structure with the first and last iterations of force constants at five temperatures are shown in Figure 4.8. The effect of using several iterations to converge the force constants is evident. For the cubic structure, there is some phonon softening at the Γ-point and X-point when using the first iteration and the phonon branches overlap at several temperatures at the Γ-point. Using the last iteration force constants, the modes no longer overlap and phonon softening as the temperature decreases is distinct. The phonon softening indicates a phase transition, despite the Free energy calculations being unsuccessful at predicting it.

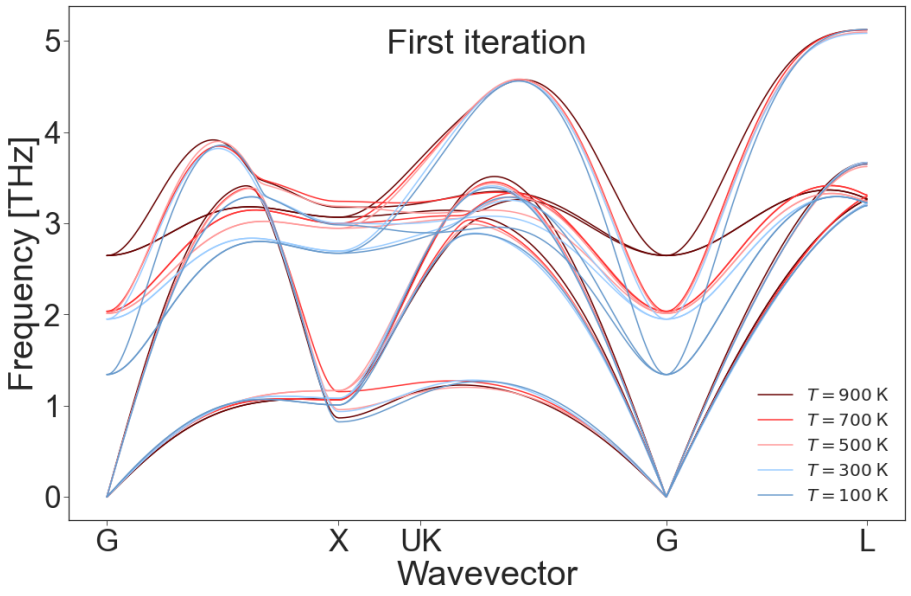

(a)

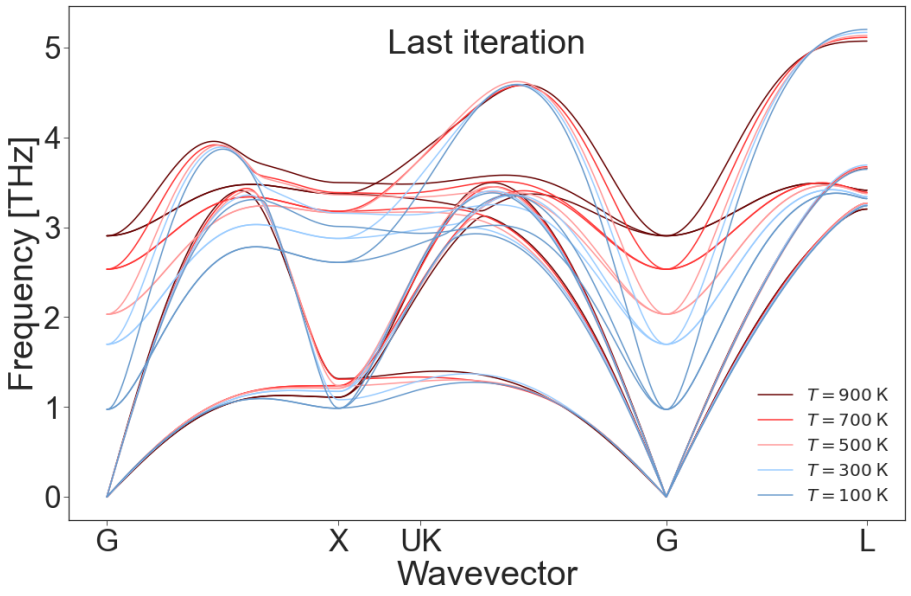

(b)

Figure 4.8: The dispersion relation for the cubic structure for 5 different temperatures with (a) first iteration force constants and (b) last iteration force constant.

The trigonal structure experiences some changes between the first and last iteration of

force constants. Where the cubic structure shows clearer softening, the phonon modes for the trigonal structure cluster together when using more iterations. The trigonal dispersion relation shows slight to no softening of the optical phonon modes at the Γ-point. As the temperature changes, the frequency also changes a little. However, this is not much compared to the cubic structure and could be caused by the high inaccuracy of the force constants. The dispersion for the trigonal structure can be viewed in Appendix C, Figure C.1.

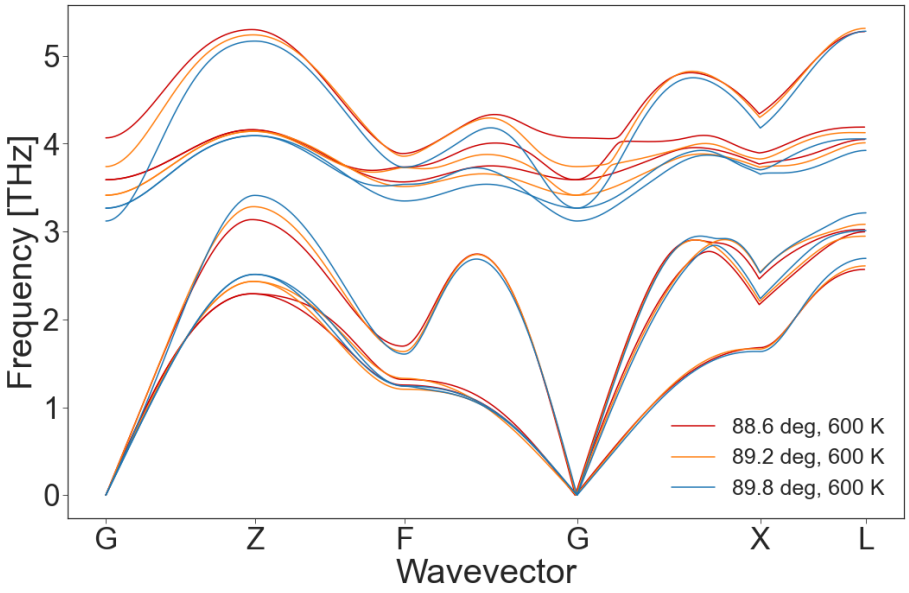

Figure 4.9: The phonon dispersion relation for the trigonal structure at three different cell shapes and constant volume. The calculations are at a temperature $T = 600$ K.

Figure 4.9 shows the phonon dispersion relations for the trigonal structure when changing the angle towards $\alpha = 90°$. The dispersion relations are calculated at $T = 600$ K. When the angle goes to 90° there is a slight softening of the optical phonons at the Γ-point.

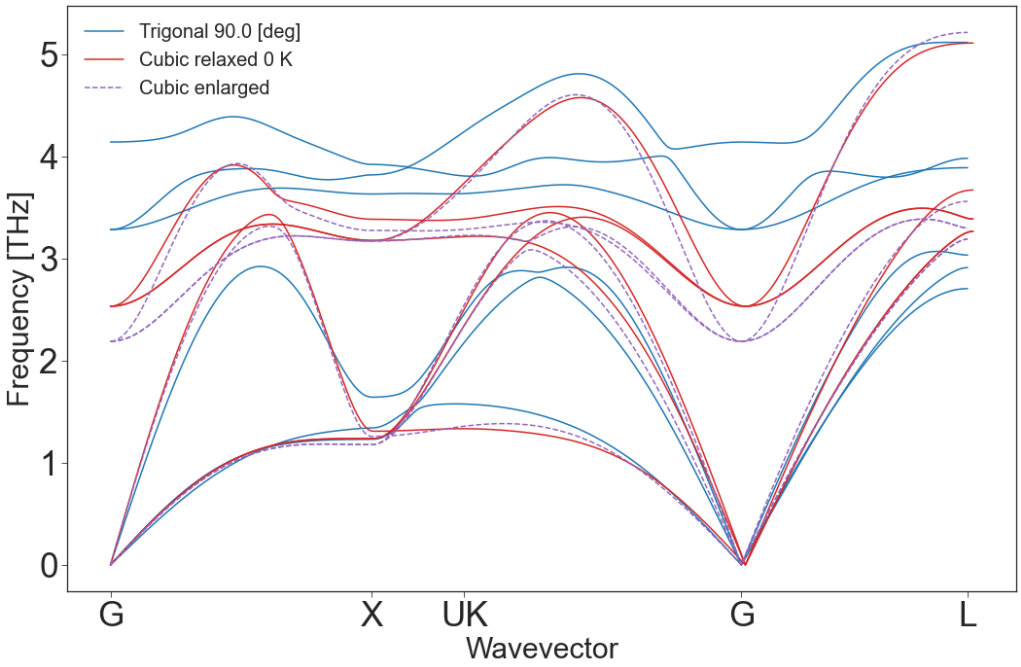

Figure 4.10: The dispersion relation of the trigonal structure with angle $\alpha = 90°$ (red), and the relaxed (blue) and enlarged (purple) cubic structures. The calculations were made at $T = 700$ K.

There is a large difference between the dispersion relation for the trigonal structure at $\alpha = 90°$ and the cubic structures. A comparison of the dispersion relations at $T = 700$ K for two sizes of the cubic and the trigonal structures at 90° has been made in Figure 4.10. The shape of the phonon modes is not corresponding to each other, which can be seen at the X-point and Γ-point.

The dissimilarity between the trigonal and cubic dispersion relations, despite having the same volume, might be due to the atomic positions in the different supercells. As mentioned in Section 4.1, the atomic positions for the trigonal cells are not the same as for the cubic cells, though the cell shapes and volume are the same. This indicates that the phonons are very sensitive to the atomic positioning in the unit cell.

The enlarged cubic cell experienced more phonon softening compared to the fully relaxed structure, illustrated in Figure 4.10. Again, confirming the importance of thermal expansion.

4.4 Phonon dispersion relation with broadening

The phonon dispersion relation with broadening, meaning the inclusion of anharmonicity, at $T = 700$ K is shown in Figure 4.11. The general shapes of the dispersion relations are still the same, but there are areas in which the phonon modes experience broadening. This indicates anharmonicity in the phonon modes. Some areas with much broadening can be seen between the U/K and Γ points and at the L point for the cubic structure.

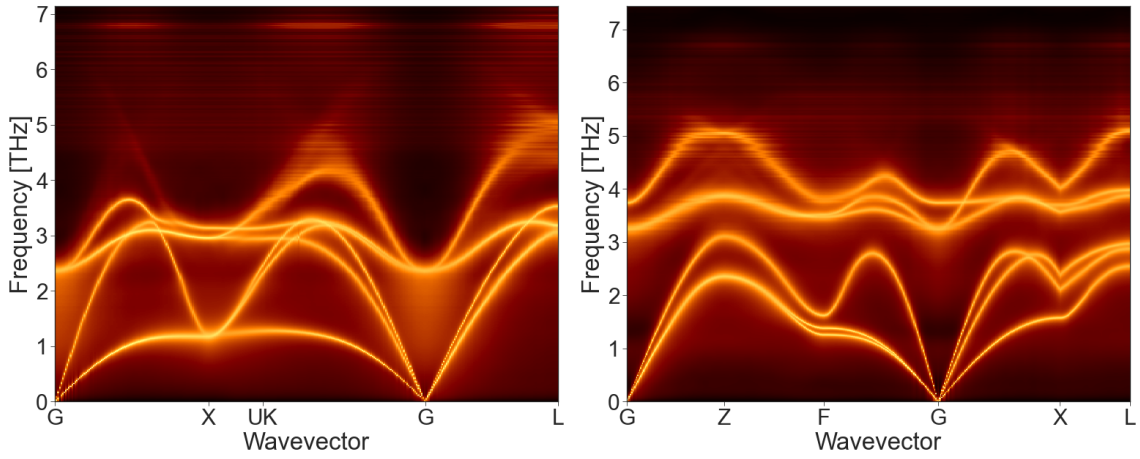

(a) Cubic structure

(b) Trigonal structure

Figure 4.11: The phonon dispersion relation plot with smearing for the (a) cubic and (b) trigonal phase of GeTe. The calculations were made at $T = 700$ K.

At the Γ-point for the cubic structure, there is a large area under the optical modes with broadening. This is also the area where the cubic structure is experiencing softening. The broadening of the dispersion relation means that the phonons scatter more easily, causing the lifetime of the phonons to shorten. This is wanted for thermoelectric materials. There is less broadening for the trigonal structure compared to the cubic.

Chapter 5

Discussion

5.1 Evaluation of the computational methods

The calculations in this thesis were made with density functional theory (DFT) and temperature dependent effective potential (TDEP) in VASP. There are several aspects of the methods that can give rise to inaccuracies in the results. Some of this inaccuracy comes from the numerical parameters discussed in Section 3.5. This and other sources of uncertainty from the method will be discussed in this section.

5.1.1 Functionals

The results show that different functionals yield different trigonal unit cell shapes. Both the volume and the angle varies depending on the functional. The chosen functional for this thesis, the vdW-DF-cx functional, corresponds less to the experimentally found angle at room temperature, compared to the PBE functional. Since parts of this thesis are focused on examining the effect of the temperature-induced angle change, choosing the vdW-DF-cx functional over the PBE functional may have introduced some errors in the calculations.

It is difficult to determine the specific consequences of choosing one functional over another. Although the volume of the PBE calculated trigonal cell is much larger than the experimentally found volumes, the correctness of the angle might have enabled a better investigation of the effect of the trigonal angle. Then again, the volume has been shown to be very important when calculating the Free energy. There may be a tradeoff between the exchange-correlation functionals since none can precisely approximate the GeTe system. Some give good results for angle changes and others are better at volume changes. Without making the same calculations for all functionals, it is difficult to say which effect they have.

5.1.2 Changing the angle

The contour plots in Figure 4.2 shows that the energy surface is not mirrored around 90°. This is due when changing the angle, the atomic positions were not manually adjusted together with the cell shape. The intention of changing the trigonal unit cell shape was for the atoms to reach their ideal positions within the cell through relaxing in VASP while maintaining the wanted shape. This did not go as expected.

At angles $\alpha > 90°$, the atomic positions did not relax to their optimal positions within the unit cells, as seen in Table 4.2. The distances between the Ge and Te atoms in the trigonal unit cells are not equal at the angles $\alpha = 90° \pm 2°$. A plausible explanation is

that the positions that have been found, are local minimums. In order to move the atoms from a local to a global minimum, the energy of the system needs to increase. This is not something automatically done in VASP. The energies calculated at $\alpha > 90°$ have not been calculated at the energetically lowest atomic positions in the unit cell.

An illustration of the atomic positions in a unit cell with $\alpha < 90°$ and a unit cell with $\alpha > 90°$ can be seen in Figure 5.1. When $\alpha < 90°$ the atoms are placed along the long diagonal, and when the angle is $\alpha > 90°$ the atoms are placed along the short diagonal. This difference in atomic placement in the cell will consequently give different energies and lattice properties.

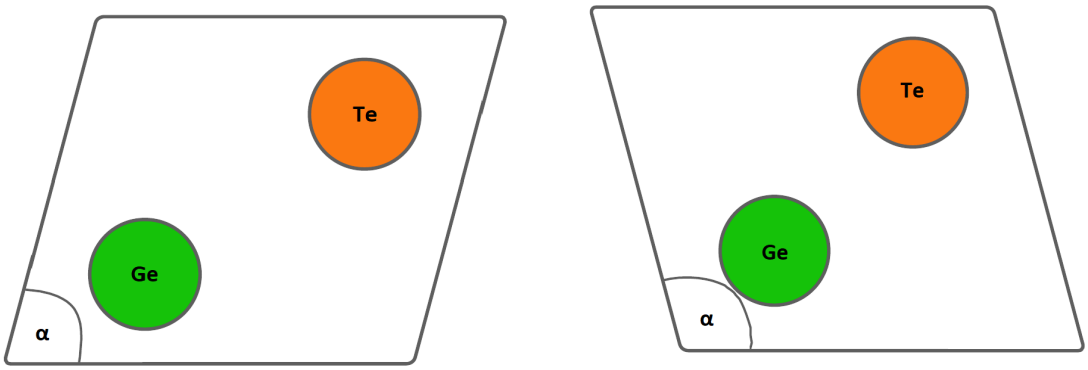

(a) $\alpha < 90°$ (b) $\alpha > 90°$

Figure 5.1: Illustration of how the atoms in the trigonal unit cell have not moved when the shape of the cell is changed. α is the angle. The green circle is Ge, while the orange is Te.

Another consequence of not manually changing the atomic positions is that the trigonal structure at $\alpha = 90°$ does not have the same atomic positions as the cubic cell. This explains the differences in the dispersion relation when comparing the cubic cells and the trigonal cell at $\alpha = 90°$. Again, VASP is unable to reach the desired atomic positions as the energy needs to go up in order to find another minimum. An illustration visualising how the cubic structure and trigonal structure at 90° differ from each other can be seen in Figure 5.2.

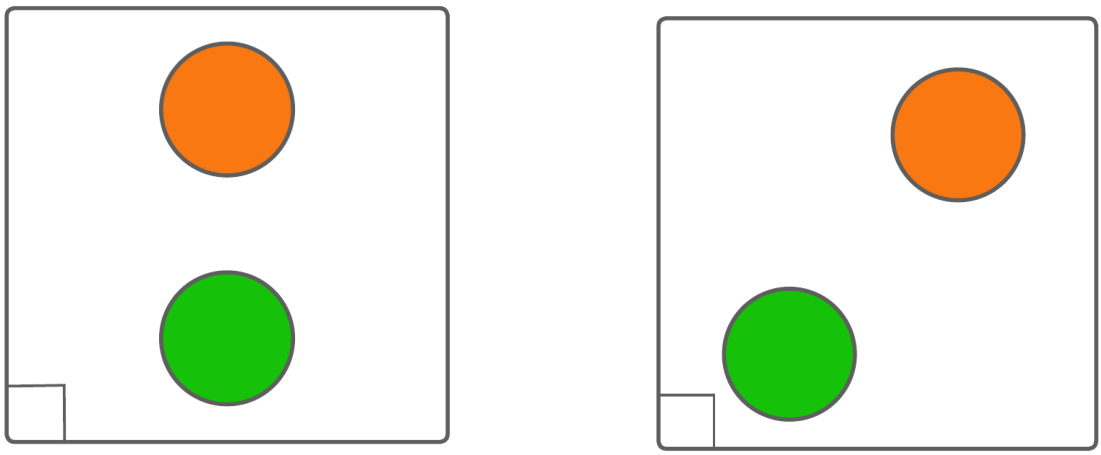

(a) Cubic structure

(b) Trigonal structure at $\alpha = 90°$

Figure 5.2: Illustration over the atomic positions in the (a) cubic unit cell and (b) trigonal unit cell with an angle $\alpha = 90°$

5.1.3 Convergence of the force constants

The effects of having converged the force constants through iterations emphasise the importance of high numerical precision when working with phonons and Free energy. Insufficient numerical precision can cause wrong results, or experimentally observed results for the wrong reasons. This is evident from the phase transition not being found when using the last iteration force constants but found when using the original force constants created from the Debye temperature. The fact that the less precise force constants got the expected results could become misleading if not investigated properly. Getting precise force constants is necessary to accurately describe the GeTe compound.

Converging the force constants reduced the uncertainty of the calculations. Unfortunately, due to the time constraints for this study, the force constants only reached a convergence of $\Delta F = 0.5$ meV/atom. This uncertainty might be one of the reasons that the R^2-scores calculated in Section 4.2.2 range from 0.23 to 0.88. The energy differences between the angles are so small that the uncertainty can have a significant effect on the results.

The number of iterations needed to converge the force constants varies. Looking at the convergence trends in Figure 4.5, one can see that at higher temperatures, there is more variation. This is an indicator that force constants at higher temperatures need more iterations to converge. This is probably the reason it required very few iterations at $T = 500$ K to reach a convergence of $\Delta F = 0.5$ meV/atom, compared to the needed iterations at $T = 700$ K, as seen in Appendix B.

The temperature has an impact, not only on the convergence rate of the force constants but also on the agreement between the approximated force constants derived from the Debye temperature and the actual force constants. For both the trigonal and the cubic structures, the difference between the first and second iterations increases with temperature as seen in Figure 4.5. At $T = 100$ K the force constants are almost converged instantly, but at higher temperatures, this is not the case. Temperature $T = 900$ K has a Free energy difference above $\Delta F = 1.5$ meV/atom between the first two iterations. This indicates that using the Debye temperature for finding approximate force constants, is better at low temperatures.

One of the reasons that the Debye approximated force constants are inaccurate could be because of the value of the used Debye temperature. The calculated Debye temperatures were found to be $\theta_{\text{tri}} = 235$ K and $\theta_{\text{cub}} = 251$ K. In other studies, the Debye temperature for GeTe was reported to be 180 K [56] and 200 K [8]. Since the calculated Debye temperature is higher than previously found, this might cause the initial force constants to be imprecise.

As the iterative process was stopped before reaching adequate convergence, the uncertainty of the calculations is higher than desired. This is not as evident when doing calculations at different temperatures, since the energy difference between calculations $\Delta T = 200$ K apart is over $\Delta F = 0.1$ eV/atom. This means that an uncertainty of 0.5 meV/atom will influence the results less than for the calculations made at a single temperature.

The difference in Free energy is much smaller for calculations made at a single temperature. A high uncertainty results in there being no clear trend readable from the results. An example of this can be seen in Figure 4.7. An uncertainty of 0.5 meV/atom makes all the Free energies with angle $\alpha < 90^\circ$ be in the range of each other. It is therefore difficult to conclude something based on the calculations made with different angles.

Despite the lack of adequate convergence of the force constants to observe the effects of changing the trigonal angle, the iterative process of converging the force constants can still be considered successful and necessary. This can be seen as there are substantial changes in the results between the first and last iterations. In Figure 4.8, the dispersion relations at different temperatures go from overlapping at the Γ-point to not doing so, enabling the opportunity to look at the phonon softening in more detail. There is reason to believe that if the iterative process continued beyond what was tested in this study, the force constants would converge. Even at higher temperatures.

One downside of this method is that it is very computationally expensive and time-consuming. It is feasible to use this method for small projects like this, but it is encouraged to find other methods of getting accurate force constants for larger projects. This would both save time and resources. One such method could be machine learning. Instead of doing pure DFT calculations, machine learning could create surrogate models to speed up the process. One such method is the Gaussian approximation potential (GAP). This has previously been done in several studies [39, 56, 57].

5.1.4 Volume considerations

When the temperature and pressure in a system change, the volume of that system might also change. Both positive and negative thermal expansion has been found theoretically and experimentally for GeTe in addition to an angle change [9, 13, 58]. Though this study did not include thermal expansion and reduction of GeTe, one calculation at $T = 700$ K with an enlarged volume compared to the ground state found cubic structure was performed. The volume was adjusted to be the same as for the trigonal structure. The results show a large difference in Free energy between the cubic structures. Since the volume was chosen not to be included in this project, there are bound to be some errors due to this.

To capture the effect of thermal expansion and angle increase when approaching the phase transition, a grid search with various temperatures, angles and volumes has been found to be necessary for Free energy calculations. When looking at the calculations of angle as a function of volume in Figure 4.3, one can see that the angle becomes smaller when the volume increases. This means that if calculations were chosen to be made with either experimental volume or angle as the basis and the other variable could relax freely, the

opposite effect of what has been experimentally found would happen. There is no simple "solution" to include both angle and volume changes.

5.2 Phase transition

A phase transition between the trigonal and cubic phase of GeTe was not found in this study. From the preceding discussion, there is reason to believe that if all degrees of freedom, temperature, angle, atomic positions and volume, were to have been included in this method, a phase transition would have been found.

The enlarged cubic cell, with a matching volume to the trigonal cells, had Free energy under the baseline of the fully relaxed trigonal structure at 0 K. This means that, if the volume of the cubic structure had expanded to become the same as the volume of the trigonal structure when increasing the temperature, a phase transition would have been found. A phase transition occurring from the thermal expansion of the cubic structure is under the assumption that the volume of the trigonal cell is constant at all temperatures.

The volume of the trigonal GeTe phase is not constant. Researchers have found in experiments and through modelling that the volume both has a positive and negative thermal expansion when approaching the phase transition temperature from 0 K in addition to the trigonal structure becoming more cubic [13, 55, 58]. The negative thermal expansion occurs when nearing the phase transition. As no calculations have been made for the trigonal structure with different volumes, it is difficult to say how much the volume impacts the Free energy and which volume is ideal at certain temperatures. More thorough calculations need to be made, to decide whether this method is capable of finding a phase transition when taking volume into consideration. To do this, the number of calculations needed would increase substantially.

Observing the effects of changing the trigonal cell to a more cubic shape became more complicated than initially anticipated. To make a reliable statement about the Free energy when changing the cell shape, the precision of the calculations needs to be high. Figure 4.6 illustrates the slight energy difference between the Free energies for the trigonal cell as a function of the angle. The precision required to draw conclusions from the results was not attained for the angle calculations. It is therefore difficult to say which effect a change in angle has on the Free energy for this GeTe system, though some changes have been seen.

Nonetheless, in the calculations with the highest R^2-score, at $T = 600$ K, the found equilibrium was closer to the cubic structure, compared to the fully relaxed trigonal structure at 0 K. This means that the method is capable of capturing some of the characteristics of GeTe. Regrettably, not to a significant extent.

It has previously been found that GeTe experiences a first-order phase transition [9]. Because of the inaccuracy in the calculations, this could not be confirmed in the present study. With better-converged force constants and all degrees of freedom taken into consideration, it could be possible to find out how and where the phase transition happened. The phase change would then perhaps be indicated by phonon softening of both the cubic and trigonal structures when approaching the critical temperature.

5.3 Phonon dispersion relation

The results show that the cubic phase of GeTe is experiencing phonon softening of the optical phonon modes around the Γ and X points as the temperature decreases. This corresponds well with previous studies [8, 9, 10]. The softening of the cubic structure as the temperature decreases is also corresponding well with the assumption that GeTe is experiencing a phase transition.

From the dispersion relations, one can see that the cubic cells calculated at $T = 700$ K are significantly different from the trigonal cell with an angle $\alpha = 90°$. The general shape of the dispersion is the same, but apart from that, the differences are relatively large. This can be seen in Figure 4.10. The cubic unit cells are experiencing clear softening, while the trigonal structure at 90° does not. This is another indicator that not manually moving the atomic positions when changing the trigonal unit cell, might have been an oversight. The trigonal cell should have been identical to the enlarged cubic cell, as the shape and volume are the same. This emphasises that atomic positions are very important in phonon calculations.

Not including all degrees of freedom when doing calculations has made a thorough investigation of the dispersion relation at the phase transition difficult. The observations made by Đorđe Dangić et al. [8, 9] that there is much softening of the trigonal structure near the phase transition and that the softening is happening as the temperature increases are not found in this study. There are no significant changes to the calculated trigonal dispersion giving indications that a phase transition occurs. This is despite the cubic structure clearly experiencing softening. Thermal expansion, angle, atomic positions and temperature is therefore important to include when calculating the trigonal structure of GeTe, again emphasising the complexity of the problem.

Lattice thermal conductivity

When looking at the broadening for the dispersion relation in Figure 4.11, one can see that there is much broadening at the Γ-point for the cubic structure. With much phonon broadening, scattering increases and the lifetime of the phonons is shorter. The result of this is that the crystal lattice transports less heat. This is highly preferable for thermoelectric materials, as short lifetimes lower the lattice thermal conductivity seen in equation 2.16.

Engineering of GeTe could be used to move the critical temperature, and therefore the phonon softening, towards room temperature. Doing so could enable GeTe to improve its thermoelectric abilities at room temperature, as stated in the paper by Subhajit Roychowdhury et al.[15]. This would be preferable for everyday applications.

5.4 Further work

There are several aspects of this study that can be improved further. The phase transition occurring in GeTe has been previously found, both theoretically and experimentally. With some adjustments to the method applied in this study, it might be possible to find the phase transition and the critical temperature. Potentially finding the critical temperature makes it easier to further see how the phonons around the critical temperature impact the lattice thermal conductivity for GeTe.

In order to find the phase transition, the inclusion of the thermal expansion for the cubic and trigonal structures can have a significant effect. Changing the volume, and therefore including one more degree of freedom, will enable the opportunity to see which crystal structure is the most energetically stable at which temperatures. Additionally, incorporating the atomic positions in the unit cells during the modification of the trigonal cell shape aids in identifying the global minima in the potential energy surface. Including atomic positions is also important, since phonons are sensitive to atomic positions.

Including thermal expansion and atomic positions in addition to the temperature and trigonal angle, would greatly increase the number of needed calculations. If all the calculations were to be calculated using the method described in this study, it would be very computationally expensive and time-consuming. Finding other methods to obtain force constants in a less computationally expensive way, could be advantageous. If the accuracy of the iteratively found force constants is high enough, it might even be possible to interpolate them. This will lower the number of calculations needed to be made and the calculated grid could be much denser.

The iterative method of finding force constants itself can also be improved. By automating the process for converging the force constants, one can make sure that all force constants are properly converged. In that way, the uncertainty of the calculations would go down. The number of iterations needed to be made for each temperature, volume and angle, would also be adjusted, so that the calculations at lower temperatures would stop earlier than the calculations at higher temperatures. This would reduce the computational cost where it is possible.

Lastly, the calculation of the lattice thermal conductivity itself would be interesting to find in future studies. By doing so, it would be easier to draw connections between the angle change, phonon dispersion relation and lattice thermal conductivity altogether.

Chapter 6

Conclusion

The aim of this thesis was to find the phase transition taking place in GeTe and examine the phonon dispersion relation as the material is transitioning from the trigonal to the cubic structure. Two types of calculations were made. The first was to use the ground state calculated unit cells for making calculations at finite temperatures. The other set of calculations was on the trigonal structure, while keeping the volume constant, the angle was changed so that the trigonal cell shape became more cubic. The vdW-DF-cx functional was used for the calculations as this functional corresponded the best with experimentally found trigonal volumes and angles.

The thermal expansion of the volume and manually changing the atomic positions in the unit were not included in this study. The results have shown that the inclusion of these parameters would have had a significant effect on the results, as neither the phase transition nor precise enough phonon dispersion relations were found without them. For the Free energy calculations, the volume was found to be an important parameter. The result shows how an enlarged cubic volume lowers the Free energy considerably. This suggests that the inclusion of thermal expansion could result in finding the phase transition.

The atomic positions in the trigonal unit cell were found to be important when calculating the dispersion relation. Because phonons arise from collectively vibration atoms, it makes sense that the distances between them are important. Unfortunately, because the atomic positions were not ideal this resulted in the phonon dispersions not being able to fully explain the behaviour of the phonons at the phase transition.

The result shows that the cubic structure experiences phonon softening and broadening at $T = 700$ K. This indicates that a phase transition is occurring in GeTe and that the phase transition could be one of the reasons for the low lattice thermal conductivity. There was no softening found for the trigonal structure with the reason probably being that the calculations surrounding the trigonal phase of GeTe are highly complex.

High precision for the calculated force constants has also been found to be significant. Although the method applied in this study is computationally expensive and time-consuming, the force constants found through the iterative process improved the results. Lowering the uncertainty by using more iterations and including all degrees of freedom, such as temperature, angle, volume and atomic positions, would increase the complexity of the calculations. However, this also increases the possibility of gaining a better understanding of the phase transition of GeTe and why it is a good thermoelectric material

Investigation of the trigonal and cubic structures of GeTe at the phase transition can give an understanding of why it is a good thermoelectric material. A greater understanding of material properties and functions can lead to further optimisation. Additionally, GeTe is probably not the only thermoelectric material experiencing good thermoelectric properties because of a phase transition. By knowing how GeTe works, one can apply this to other materials and open up the scope for perhaps finding new and better materials with similar thermoelectric properties.

Bibliography

[1] *What are the Least Developed Countries?* Last accessed 27 January 2023 from the United Nations Conference. 2022. URL: https://unctad.org/press-material/what-are-least-developed-countries-8t.

[2] D. S. Arar. *Thermocouple Principles—the Seebeck Effect and Seebeck Coefficient.* Last accessed 18 January 2023. 2022. URL: https://www.allaboutcircuits.com/technical-articles/thermocouple-principles-seebeck-effect-seebeck-voltage-seebeck-coefficients/.

[3] N. Yogesh, S. Omkar, and G. G. abd Ghorpade Omkar. "Air Conditioning System in Car using Thermoelectric Effect". In: *International Journal of Engineering Research & Technology* 9 (2020). DOI: https://doi.org/10.1002/anie.200900598.

[4] G. J. Snyder and E. S. Toberer. "Complex thermoelectric materials". In: *Nature Materials* 7 (2008). URL: https://doi.org/10.1038/nmat2090.

[5] G. P. Srivastava. *The Physics of Phonons.* IOP publishing Ltd, 1990.

[6] J. R. Sootsman, D. Y. Chung, and M. G. Kanatzidis. "New and Old Concepts in Thermoelectric Materials". In: *Angewandte Chemie International Edition* 48 (2009). DOI: https://doi.org/10.1002/anie.200900598.

[7] D. S. Sholl and J. A. Steckel. *Density Functional Theory: A Practical Introduction.* John Wiley & Sons Singapore Pte. Ltd, 2009.

[8] Đ. Dangić et al. "The origin of the lattice thermal conductivity enhancement at the ferroelectric phase transition in GeTe". In: *npj Computational Materials 2021 7:1* 7 (2021). DOI: 10.1038/s41524-021-00523-7.

[9] Đ. Dangić, S. Fahy, and I. Savi ć. "Molecular dynamics simulation of the ferroelectric phase transition in GeTe: Displacive or order-disorder character". In: *Phys. Rev. B* 106 (2022). DOI: 10.1103/PhysRevB.106.134113.

[10] U. D. Wdowik et al. "Soft-phonon mediated structural phase transition in GeTe". In: *Physical Review B - Condensed Matter and Materials Physics* 89 (2014). DOI: 10.1103/PhysRevB.89.224306.

[11] S. A. J. Kimber, J. Zhang, and C. H. L. et al. "Dynamic crystallography reveals spontaneous anisotropy in cubic GeTe". In: *Nature Materials* 22 (2023). DOI: 10.1038/s41563-023-01483-7.

[12] A.-K. U. Michel et al. "Phase transitions in germanium telluride nanoparticle phase-change materials studied by temperature-resolved x-ray diffraction". In: *Journal of Applied Physics* 129 (2021). DOI: 10.1063/5.0032624.

[13] T. Chattopadhyay, J. X. Boucherle, and H. G. von Schnering. "Neutron diffraction study on the structural phase transition in GeTe". In: *Journal of Physics C: Solid State Physics* 20 (1987). DOI: 10.1088/0022-3719/20/10/012.

[14] O. Yarema et al. "Colloidal Phase-Change Materials: Synthesis of Monodisperse GeTe Nanoparticles and Quantification of Their Size-Dependent Crystallization". In: *Chemistry of Materials* 30 (2018). DOI: doi:10.1021/acs.chemmater.8b02702.

[15] S. Roychowdhury et al. "Germanium Chalcogenide Thermoelectrics: Electronic Structure Modulation and Low Lattice Thermal Conductivity". In: *Chemistry of Materials* 30 (2018). DOI: 10.1021/ACS.CHEMMATER.8B02676.

[16] Y. Wnag et al. "First-principles calculations of lattice dynamics and thermal properties of polar solids". In: *Computational Materials* 2 (2021). DOI: 10.1038/npjcompumats.2016.6.

[17] C. Kittel. *Introduction to solids state physics*. 8th ed. John Wiley & Sons Singapore Pte. Ltd, 2015.

[18] P. Raja and A. Barron. *Crystal Structure*. Last accessed 23 April 2023. 2022. URL: https://chem.libretexts.org/@go/page/55904.

[19] G. Sosso et al. "Neural network interatomic potential for the phase change material GeTe". In: *Physical Review B* 85 (2012). DOI: 10.1103/PhysRevB.85.174103.

[20] T. E. o. E. Britannica. *Space group*. Last accessed 23 April 2023. Sept. 2022. URL: https://www.britannica.com/science/space-group.

[21] *Reciprocal space*. Last accessed 08 April 2023, from University of Cambridge. URL: https://www.doitpoms.ac.uk/tlplib/reciprocal_lattice/printall.php.

[22] Tasci, E.S. et al. "An introduction to the tools hosted in the Bilbao Crystallographic Server". In: *Acta Cryst* 70 (2014). DOI: 10.1051/epjconf/20122200009.

[23] Aroyo, M.I. et al. "Brillouin-zone database on the Bilbao Crystallographic Server". In: *EPJ Web of Conferences* 22 (2012). DOI: doi:10.1107/S205327331303091X.

[24] J. Garai. "Physics behind the Debye temperature". In: *arXiv: Chemical Physics* (2007).

[25] B. Wei et al. "Phonon anharmonicity: a pertinent review of recent progress and perspective". In: *Science China Physics, Mechanics, and Astronomy* 64 (2021). DOI: 10.1007/s11433-021-1748-7.

[26] G. Venkataraman. "Soft modes and structural phase transitions". In: *Bulletin of Materials Science* 1 (1979). DOI: 10.1007/BF02743964.

[27] K. Daniel I. *Basic Aspects of the Quantum Theory of Solids : Order and Elementary Excitations*. Cambridge University Press, 2010. URL: https://search.ebscohost.com/login.aspx?direct=true&db=e000xww&AN=329395&site=ehost-live.

[28] Y. Mo and I. Szlufarska. "Nanoscale heat transfer: Single hot contacts". In: *Nature materials* 12 (2012). DOI: 10.1038/nmat3506.

[29] C. Persson. *Brief introduction to the density functional theory*. 2022.

[30] J. Ismael. *Quantum Mechanics*. Ed. by T. S. E. of Philosophy. Last accessed 24 April 2023. 2021. URL: https://plato.stanford.edu/archives/fall2021/entries/qm/.

[31] *Quantum mechanics*. Last accessed 24 April 2023 from Oxford English Dictionary. 2022. URL: https://www.oed.com/view/Entry/155942?redirectedFrom=Quantum+mechanics&.

[32] J.-P. Hannsen. *Kvantemekanikk*. Last accessed 21 April 2023. 2021. URL: https://snl.no/kvantemekanikk.

[33] O. Hellman and N. Shulumba. *Temperature dependent effective potential*. Last accessed 31 March 2023. URL: https://ollehellman.github.io/index.html.

[34] O. Hellman, I. A. Abrikosov, and S. I. Simak. "Lattice dynamics of anharmonic solids from first principles". In: *Phys. Rev. B* 84 (2011). DOI: 10.1103/PhysRevB.84.180301.

[35] O. Hellman and I. A. Abrikosov. "Temperature-dependent effective third-order interatomic force constants from first principles". In: *Phys. Rev. B* 88 (2013). DOI: 10.1103/PhysRevB.88.144301.

[36] O. Hellman et al. "Temperature dependent effective potential method for accurate free energy calculations of solids". In: *Phys. Rev. B* 87 (2013). DOI: 10.1103/PhysRevB.87.104111.

[37] R. A. Tranås. *Identifying Materials With Low Lattice Thermal Conductivity Using Machine Learning and Computational Modeling*. 2023.

[38] N. Shulumba. "Vibrations in solids From first principles lattice dynamics to high temperature phase stability". In: *Linköping University Electronic Press* (2015). DOI: 10.3384/diss.diva-122949.

[39] S. Bichelmaier. *Ab-initio modelling of material properties using elements of artificial intelligence*. 2023.

[40] O. Hellman and N. Shulumba. *Canonical configuration*. Last accessed 17 April 2023. URL: https://ollehellman.github.io/program/canonical_configuration.html.

[41] G. Kresse and J. Hafner. "Ab initio molecular dynamics for liquid metals". In: *Phys. Rev. B* 47 (1993). DOI: 10.1103/PhysRevB.47.558.

[42] G. Kresse and J. Furthmüller. "Efficiency of ab-initio total energy calculations for metals and semiconductors using a plane-wave basis set". In: *Computational Materials Science* 6 (1996). DOI: https://doi.org/10.1016/0927-0256(96)00008-0.

[43] G. Kresse and J. Furthmüller. "Efficient iterative schemes for ab initio total-energy calculations using a plane-wave basis set". In: *Phys. Rev. B* 54 (1996). DOI: 10.1103/PhysRevB.54.11169.

[44] A. H. Larsen et al. "The atomic simulation environment—a Python library for working with atoms". In: *Journal of Physics: Condensed Matter* 29 (2017). DOI: 10.1088/1361-648X/AA680E.

[45] F. Pedregosa et al. "Scikit-learn: Machine Learning in Python". In: *Journal of Machine Learning Research* 12 (2011), pp. 2825–2830.

[46] A. Jain et al. "Commentary: The Materials Project: A materials genome approach to accelerating materials innovation". In: *APL Materials* 1 (2013). DOI: 10.1063/1.4812323.

[47] VASP-manual. *KPOINTS*. Last accessed 18 April 2023. URL: https://www.vasp.at/wiki/index.php/KPOINTS.

[48] G. Kresse and D. Joubert. "From ultrasoft pseudopotentials to the projector augmented-wave method". In: *Phys. Rev. B* 59 (1999). DOI: 10.1103/PhysRevB.59.1758.

[49] J. P. Perdew, K. Burke, and M. Ernzerhof. "Generalized Gradient Approximation Made Simple". In: *Phys. Rev. Lett.* 77 (1996). DOI: 10.1103/PhysRevLett.77.3865.

[50] J. P. Perdew et al. "Restoring the Density-Gradient Expansion for Exchange in Solids and Surfaces". In: *Phys. Rev. Lett.* 100 (2008). DOI: 10.1103/PhysRevLett.100.136406.

[51] J. Sun, A. Ruzsinszky, and J. P. Perdew. "Strongly Constrained and Appropriately Normed Semilocal Density Functional". In: *Phys. Rev. Lett.* 115 (2015). DOI: 10.1103/PhysRevLett.115.036402.

[52] K. Berland and P. Hyldgaard. "Exchange functional that tests the robustness of the plasmon description of the van der Waals density functional". In: *Phys. Rev. B* 89 (2014). DOI: 10.1103/PhysRevB.89.035412.

[53] E. W. Weisstein. *Lorentzian Function*. Ed. by F. M.-.-A. W. W. Recource. Last accessed 21 April 2023. URL: https://mathworld.wolfram.com/LorentzianFunction.html.

[54] P. Virtanen et al. "SciPy 1.0: Fundamental Algorithms for Scientific Computing in Python". In: *Nature Methods* 17 (2020). DOI: 10.1038/s41592-019-0686-2.

[55] J. Goldak et al. "Structure of alpha GeTe". In: *The Journal of Chemical Physics* 44 (1966). DOI: 10.1063/1.1727231.

[56] D. Campi et al. "First-principles calculation of lattice thermal conductivity in crystalline phase change materials: GeTe, Sb2 Te3, and Ge2 Sb2 Te5". In: *Physical Review B* 95 (2017). DOI: 10.1103/PhysRevB.95.024311.

[57] A. P. Bartók et al. "Gaussian Approximation Potentials: The Accuracy of Quantum Mechanics, without the Electrons". In: *Phys. Rev. Lett.* 104 (2010). DOI: 10.1103/PhysRevLett.104.136403.

[58] Đ. Dangić et al. "Coupling between acoustic and soft transverse optical phonons leads to negative thermal expansion of GeTe near the ferroelectric phase transition". In: *Phys. Rev. B* 97 (2018). DOI: 10.1103/PhysRevB.97.224106.

Appendix A

PYTHON script

A.1 Changing the trigonal angle

This script shows the code used for changing the angle of the trigonal structure while holding the lattice constant constant. The code used ASE in order to change the shape. The positions of the atoms in the unit cell were not changed in the script but relaxed in VASP.

```
# Importing packages
from ase import io
from ase.build import cut, sort
import numpy as np

# Importing fully relaxed trigonal structure POSCAR-file
atoms = io.read('POSCAR')

# Centering the structure
positions = atoms.get_scaled_positions()
new_positions = [np.subtract(positions[0], positions[0]),
np.subtract(positions[1], positions[0])]
atoms.set_scaled_positions(new_positions)

# Creating a quasi-cubic supercell
sat = cut(atoms, a =(-1,1,1), b=(1,-1,1), c=(1,1,-1))

# Keeping the lattice constant constant if wanted
lat_const = sat.cell.get_bravais_lattice().a

# Input angle from the user
alpha = float(sys.argv[1])

# Changing the quasi-cubic cell shape
sat.set_cell([lat_const, lat_const, lat_const, alpha, alpha, alpha],
             scale_atoms=True)

# Cutting the cell shape down to a primitive unit cell size
at_t = cut(sat, a=(0, 1/2, 1/2), b=(1/2, 0, 1/2), c=(1/2, 1/2, 0))

# Naming according to input angle
name = 'POSCAR'+str(alpha)

# Writing a new POSCAR file adapted to VASP
io.vasp.write_vasp(name, sort(at_t),vasp5=True,direct=True)
```

Appendix B

Convergence tests

B.1 Force constants

The following figures illustrate how the force constants converged at different temperatures when changing the unit cell angle. The number of canonical configurations per iteration was four for the temperatures $T = 500$ K and 700 K and seven at $T = 600$ K.

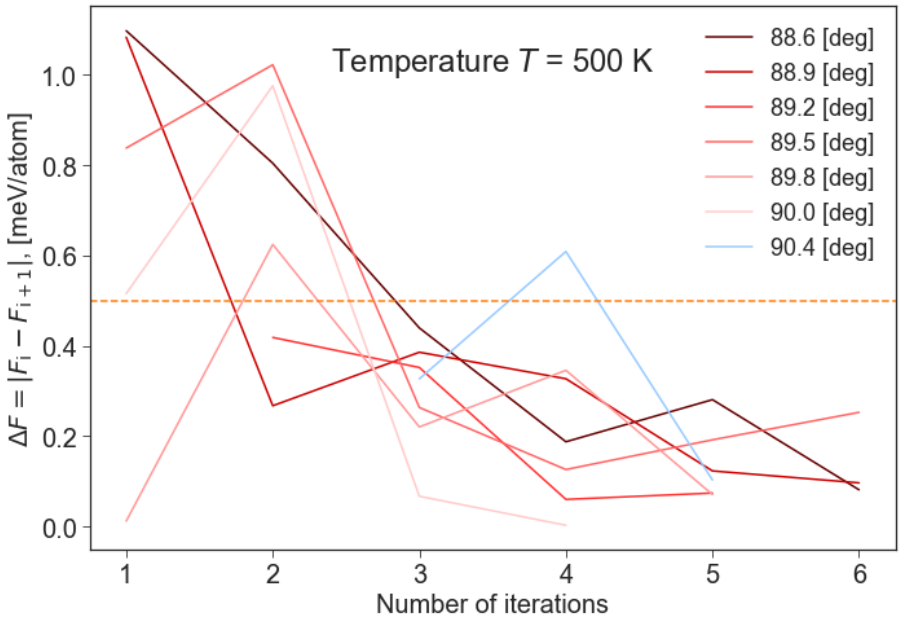

Figure B.1: Convergence of the force constants at $T = 500$ K for different angles. The orange dashed line is the threshold at $\Delta F = 0.5$ meV/atom.

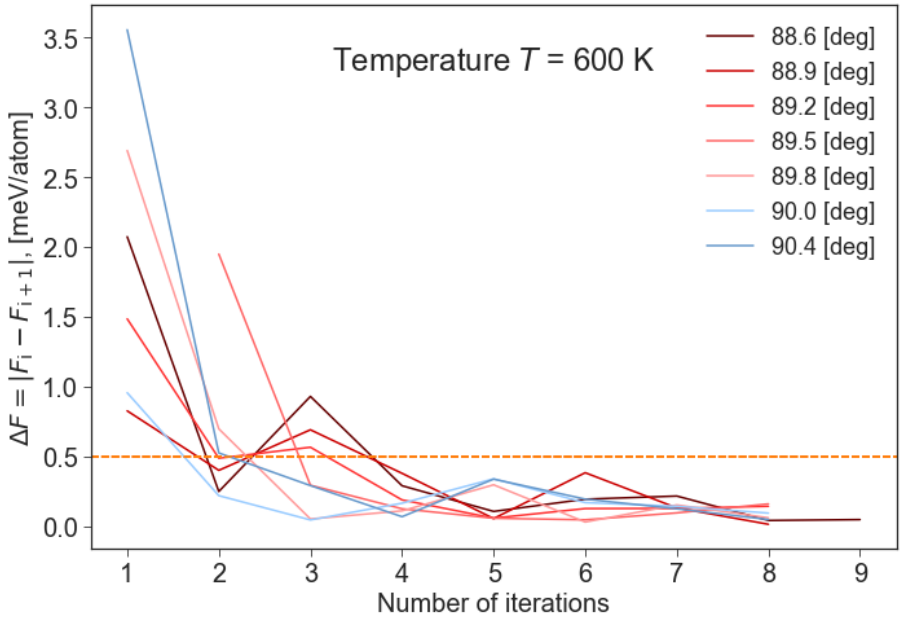

Figure B.2: Convergence of the force constants at $T = 600$ K for different angles. The orange dashed line is the threshold at $\Delta F = 0.5$ meV/atom.

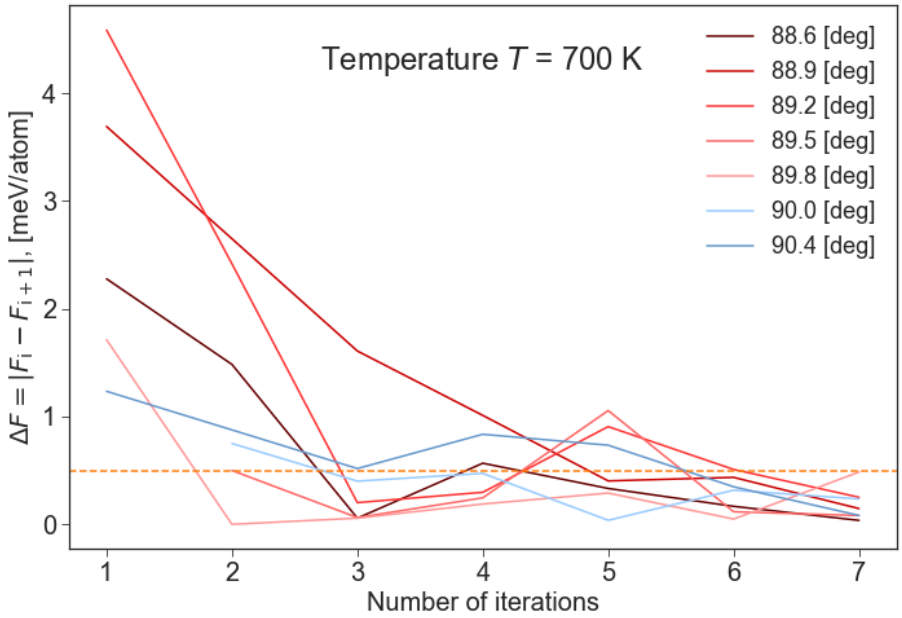

Figure B.3: Convergence of the force constants at $T = 700$ K for different angles. The orange dashed line is the threshold at $\Delta F = 0.5$ meV/atom.

Appendix C

Trigonal dispersion relation

The phonon dispersion relation for the trigonal structure, when using first and last iteration force constants.

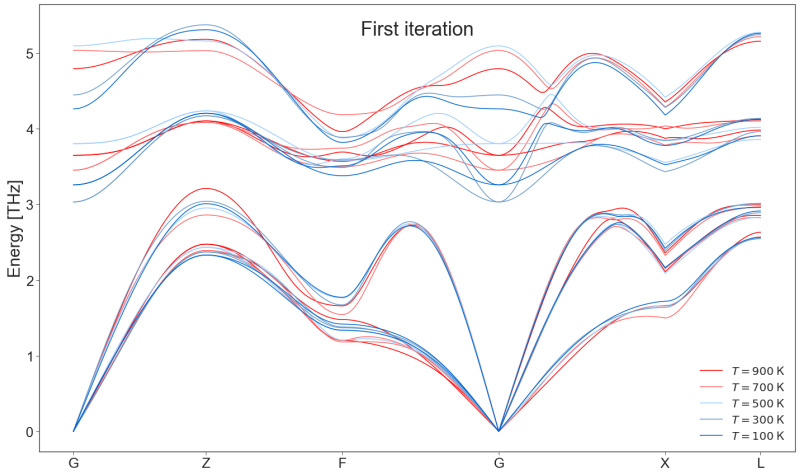

(a)

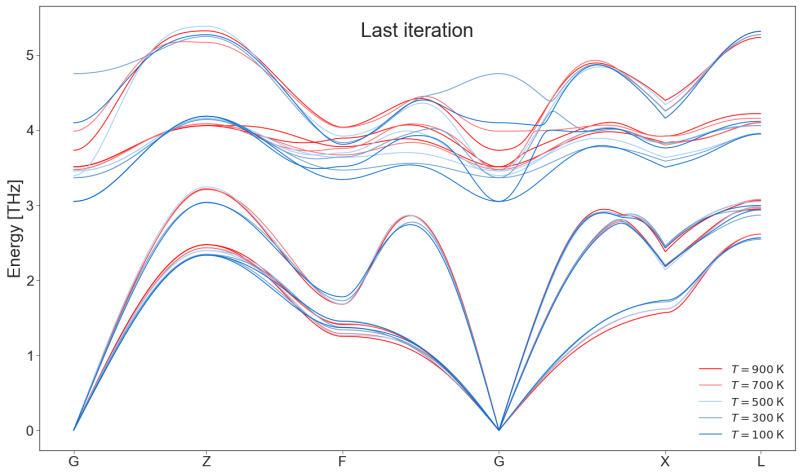

(b)

Figure C.1: The dispersion relation for the trigonal structure at 5 different temperatures with (a) first iteration force constants and (b) last iteration force constants.

Figure C.1 illustrates the effect of using more precise force constants for phonon calculations

as there is a relatively large change in the dispersions. The dispersion shows no sign of phonon softening at temperatures around the experimentally found phase transition (700 K).

Norges miljø- og biovitenskapelige universitet
Noregs miljø- og biovitskapelege universitet
Norwegian University of Life Sciences

Postboks 5003
NO-1432 Ås
Norway